Spring 2019

EXPERIMENTAL INVESTIGATION OF THE THERMOCHEMICAL REDUCTION OF ARSENITE AND SULFATE: LOW TEMPERATURE HYDROTHERMAL COPPER, NICKEL, AND COBALT ARSENIDE AND SULFIDE ORE FORMATION

Nicholas Allin

EXPERIMENTAL INVESTIGATION OF THE THERMOCHEMICAL REDUCTION OF ARSENITE AND SULFATE: LOW TEMPERATURE HYDROTHERMAL COPPER, NICKEL, AND COBALT ARSENIDE AND SULFIDE ORE FORMATION

by

Nicholas C. Allin

A thesis submitted in partial fulfillment of the
requirements for the degree of

Masters in Geoscience:
Geology Option

Montana Technological University

2019

Abstract

Experiments were conducted to determine the relative rates of reduction of aqueous sulfate and aqueous arsenite ($As(OH)_3$,aq) using foils of copper, nickel, or cobalt as the reductant, at temperatures of 150ºC to 300ºC. At the highest temperature of 300°C, very limited sulfate reduction was observed with cobalt foil, but sulfate was reduced to sulfide by copper foil (precipitation of Cu_2S (chalcocite)) and partly reduced by nickel foil (precipitation of NiS_2 (vaesite) + $NiSO_4 \cdot xH_2O$). In the 300ºC arsenite reduction experiments, Cu_3As (domeykite), Ni_5As_2, or CoAs (langisite) formed. In experiments where both sulfate and arsenite were present, some produced minerals were sulfarsenides, which contained both sulfide and arsenide, i.e. cobaltite (CoAsS). These experiments also produced large (~10 µm along longest axis) euhedral crystals of metal-sulfide that were either imbedded or grown upon a matrix of fine-grained metal-arsenides, or, in the case of cobalt, metal-sulfarsenide. Some experimental results did not show clear mineral formation, but instead demonstrated metal-arsenic alloying at the foil edges. Below 250ºC in the mixed experiments, reduction of sulfate was not observed, but reduction of arsenite by copper to form domeykite was prominent at temperatures down to at least 150ºC, and reduction of arsenite by nickel to form an un-named mineral, Ni_3As, as a crystalline crust occurred as low as 150°C. The implication is that a low temperature fluid carrying both aqueous sulfate and arsenite will quickly precipitate metal-arsenide minerals at a reducing interface, whereas sulfate reduction is much slower, especially at temperatures below 250ºC. This helps to explain the abundance of metal-arsenide minerals and relative lack of metal-sulfide minerals in certain ore deposit types, including unconformity-type U-Ni and “5-element suite” vein deposits.

Keywords: arsenic, arsenide, reduction, cobalt, thermochemical, sulfide

Dedication

I would like to dedicate this to everyone in my life who has supported me.

Acknowledgements

Here I would like to thank my advisor, Dr. Chris Gammons, and my thesis committee members Dr. Glenn Shaw, Dr. Doug Cameron, and Gary Wyss for their support and guidance. I would also like to recognize and express gratitude for all the previous research done by scientists that is publicly available. This research was partially funded by NSF Grant #1624420. Without their help, none of this would have been possible.

Table of Contents

List of Tables

List of Figures

1. Introduction

1.1. Objective

The goal of this study is to investigate the relative reaction rates of thermochemical sulfate reduction (TSR) and thermochemical arsenite ($As(OH)_{3,}aq$) reduction (TAR) at temperatures between 150°C and 300°C. In general, sulfide minerals are extremely common. Arsenide minerals, aside from arsenopyrite, are usually considered uncommon or rare. Despite this, there are certain deposits (e.g. Table I) which have a simultaneous abundance of arsenides and lack of sulfides. Both TAR, TSR, and their rates of reaction could play an important role in the formation of ore deposits like those listed in Table I.

Table I. Ore deposit districts where TAR and TSR may be important

Deposit Type	Location	Important Elements	Temperature of Formation	Exceptional Species	References
U-Ni Unconformity	Athabaska Basin, Saskatchewan, CA	U, Ni, As	<200°C	U-oxide, Ni-arsenide	Dahlkamp, 1978; Richard et al., 2013
Five-element suite	Cobalt-Gowganda, Echo Bay and Thunder Bay Districts, CA	Ni, Co, Ag, As, Bi	150-500°C	native As, Ag	Petruk, 1971; Kissin, 1992
Native Copper	Keeweenawan Peninsula, Michigan, USA	Cu, As, S	~100-250°C	Native Cu, mohawkite (CuAs)	Moore, 1962; Koenig, 1900; Brown, 2006
Red-bed Copper	Corocoro District, BO	Cu, S, As, Pb, Ag, Fe	low	Native Cu, Ag	Avila-Salinas, 1990; Ljunggren and Meyer, 1964; Cox et al., 2013

1.2. Thermochemical Sulfate Reduction (TSR)

Sulfate is a common anion (SO_4^{2-}) that is found in most near-surface environments where oxygen is plentiful. Sulfate contains oxidized sulfur, where sulfur is in the +6 valence state and bonded to oxygen in a rigid tetrahedral structure (four oxygen atoms surrounding the central sulfur atom). Reduction of sulfate happens when the sulfur atom gains *n* electrons, lowering the valence state of sulfur. The valence state of sulfur can vary between +6 to -2, and the reduction of sulfate often produces sulfur in the -2 valence state, called sulfide (S^{2-}). The reduction of sulfate to sulfide is given in the generalized reaction:

$$8e^- + SO_4^{2-}\,(aq) + 10H^+\,(aq) \rightarrow 4H_2O\,(l) + H_2S\,(g) \qquad (1)$$

where e^- are electrons.

Thermochemical sulfate reduction (TSR) plays an important role in both the petroleum and natural resource industries. In the petroleum industry, TSR contributes to the production of "sour gas", which is natural gas that contains hydrogen sulfide, H_2S (g), with sulfur concentrations between 0.005% to <0.3%, depending on conditions (Brunner and Woll, 1980). Anaerobic sulfate reducing bacteria (SRB) contribute as the largest source of sulfide below temperatures of 100°C by oxidizing hydrocarbons to reduce sulfate to sulfide gas as part of their respiration process (Barton and Tomei, 1995). In deeper reservoirs, at temperatures above 100°C, the majority of sulfide is produced by TSR reactions that are thermodynamically favored without the assistance of SRB (Barton and Tomei, 1995; Goldstein and Aizenshtat, 1994).

TSR has been thought to play some role in the formation of certain ore deposits, such as Mississippi Valley Type (MVT) deposits (Thom and Anderson, 2008). However, the formation of ore deposits by way of TSR has been debated, as the reaction rate is generally considered to be quite slow at the lower temperatures (≤200°C) found at MVT deposits (Goldstein and Aizenshtat, 1994). This can be refuted by the idea of TSR occurring over large periods of time

before the formation of an ore deposit, allowing a buildup of sulfide as H_2S (g) (equation 1) to be stored in the sedimentary formation and then reacted with the introduction of metal-rich fluids (Goldhaber and Orr, 1995). This thought may only be applicable depending on the source of sulfate. Sulfate in sedimentary formations may undergo TSR under the right conditions, allowing for H_2S (g) storage over time (Goldhaber and Orr, 1995), but many ore forming models rely on the transportation of sulfate via hydrothermal fluids (some seen in Table I), which makes H_2S (g) storage over time difficult at lower temperatures.

SRB cannot survive within the range of temperatures for the experiments conducted in this paper (150 to 300°C), so the production of sulfide from sulfate must be abiotic (Barton and Tomei, 1995; Jørgensen et al., 1992). TSR reactions, while thermodynamically favored, do not occur on timescales relevant to bench-top experiments (days to weeks) at temperatures below about 250° due to kinetic barriers (Goldstein and Aizenshtat, 1994). Above 250°C, TSR has been reproduced in the laboratory at bench-top experiment time scales (Goldstein and Aizenshtat, 1994). The temperature parameters for the experiments in this study were chosen to be above the range of SRB activity, but within possible TSR.

1.3. Thermochemical Arsenite Reduction (TAR)

Thermochemical arsenite reduction (TAR) has barely been investigated, aside from an undergraduate honors thesis where thermochemical arsenite reduction was somewhat successfully induced by elemental iron wire (Blair, 1997). In fact, the term “thermochemical arsenite reduction” and associated acronym “TAR” is not established in the literature. Because of limited published literature, not much about the reaction is understood.

Common valence states for arsenic in low temperature aqueous systems are: -3 (arsenide), 0 (arsenic), +3 (arsenite), and +5 (arsenate). In oxygen rich surficial environments,

the most prevalent species of arsenic is arsenate. In contrast, a rock-buffered hydrothermal system at temperatures within the scope of this study has the dominant form of arsenic as arsenite, or $As(OH)_{3,}aq$ (also written as $H_3AsO_3^0$) (Heinrich and Eadington, 1986). Figure 1 shows that $H_3AsO_3^0$ is the dominant aqueous species at 250°C for a hydrothermal fluid buffered near the aqueous sulfate/sulfide boundary and at pH values less than 8. To better represent these conditions, this paper and the subsequent experiments focuses on arsenite as the primary arsenic species in solution.

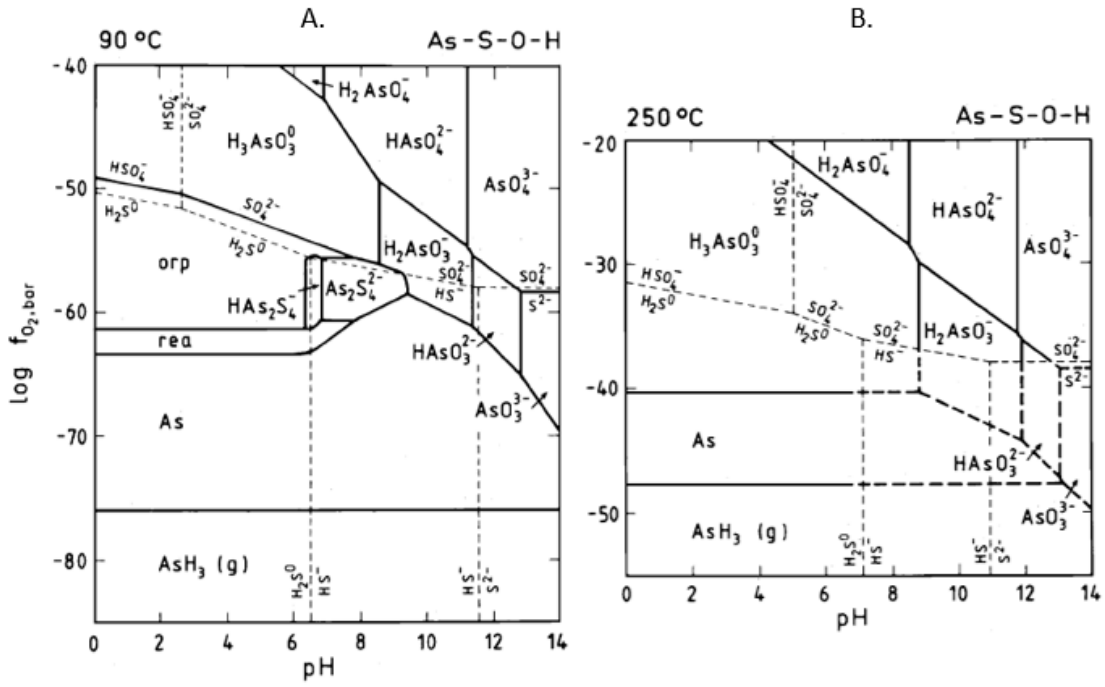

Figure 1. The As-S-O-H system in pH-log fO_2 space at temperatures between 90°C and 250°C. Modified from Heinrich and Eadington, 1986. Dashed lines show stability fields of aqueous sulfur species.

For the formation of arsenide to occur from either arsenite or arsenate, six to eight electrons respectively must be gained by the arsenic atom. The generalized reduction reaction for this is:

$$As(OH)_3\,(aq) + 6e^- + 6H^+\,(aq) \rightarrow H_3As(aq) + 3H_2O\,(l) \qquad (2)$$

or

$$H_2AsO_4^- (aq) + 8e^- + 9H^+ (aq) \rightarrow H_3As(aq) + 4H_2O (l)$$

where e^- are electrons.

A form of arsenic reduction that requires a smaller transfer of only two electrons is exploited by microbes for energy production (Escudero et al., 2013). Microbes can reduce arsenic from the +5 valence state to +3 valence state or oxidize arsenic from the +3 valence state to the +5 valence state (Escudero et al., 2013). The production of some arsenic-sulfides in surficial environments has been directly linked to microbial activity (Demergasso et al., 2007), but remains insignificant as a contributing factor to the production of minerals in this study. The temperature range of 200-150°C limits arsenide production to an abiotic process.

The same electron donors (reducing agents) that contribute to TSR could possibly be electron donors in TAR. Because the dominant form of arsenic in hydrothermal fluids is arsenite, a transfer of only six electrons is necessary, unlike the transfer of eight electrons required to reduce sulfate to sulfide in TSR. It is therefore reasonable to hypothesize that under the same conditions, if the same reducing agents in TSR could be reducing agents in TAR, then TAR could have a faster reaction rate than TSR at temperatures ≤ 300°C.

1.4. Experimental Approach

The experiments in this study use elemental copper (Cu), nickel (Ni), and cobalt (Co) as electron donors to test the relative rates of TSR and TAR in the temperature range of 150°C to 300°C. The elements Cu, Ni, and Co occur naturally as both sulfide and arsenide minerals, so formation of one or the other suite of minerals can be taken as evidence of one reaction predominating over the other. These elemental foils are easily attainable in pure (99.999%) form from scientific suppliers. A high reductive capacity is provided by the native metals through the

reduction-oxidation (redox) couples generated by the dissolution of the foils from a solid to an aqueous oxidized state (Cu/Cu^{+}, Ni/Ni^{2+}, and Co/Co^{2+}; Figure 2).

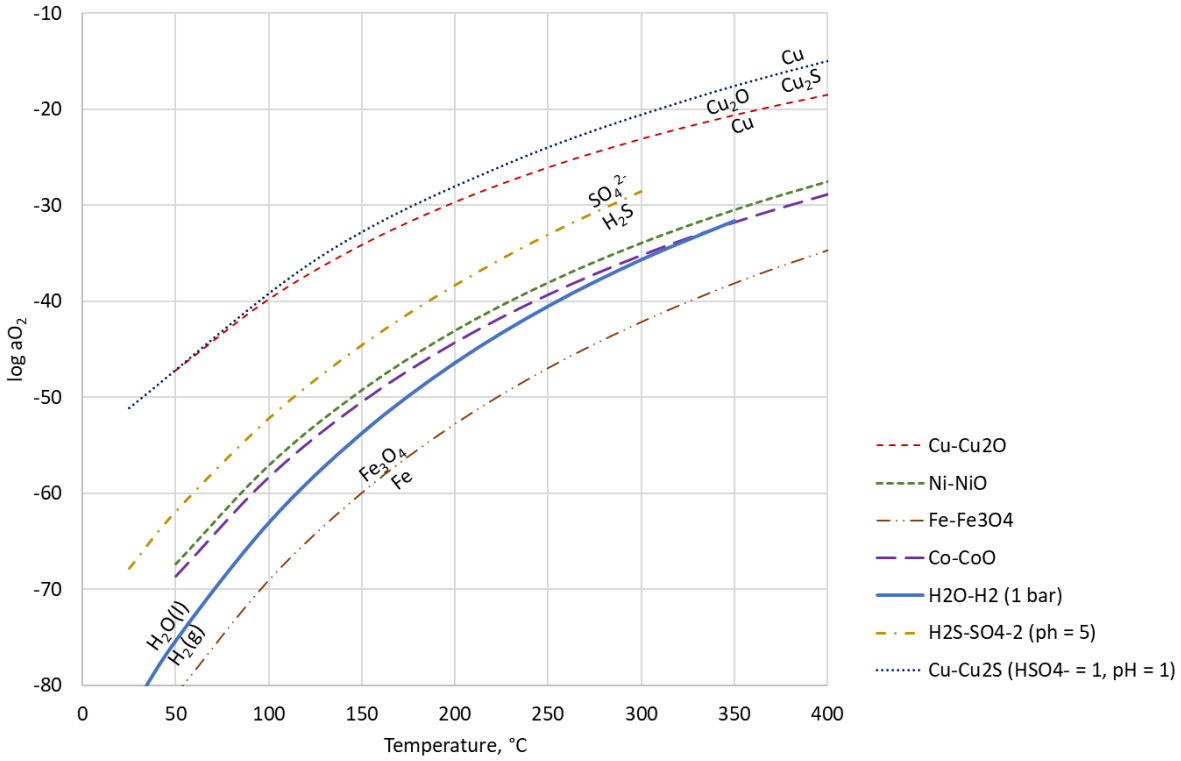

Figure 2. LogaO_2 vs temperature diagram: stability lines for the redox couples Cu-Cu_2O, Ni-NiO, Co-CoO. Fe-Fe_3O_4, H_2O-H_2, SO_4^{2-}-H_2S, and Cu-Cu_2S stability lines are represented. Thermodynamic data are from O'Neill and Pownceby, 1993; Robie et al., 1979.

There have been experimental investigations into the high temperature oxidation of these metals to their respective oxides (Cu_2O, NiO, and CoO) (O'Neill and Pownceby, 1993). From these experiments, equations for determining oxygen buffer values for these redox couples were established (O'Neill and Pownceby, 1993). Although the appropriate temperature ranges for these equations are above the temperatures performed in this study, the results are within nearly one logaO_2 unit compared to calculations using previously established standard state data (Robie et al., 1979) when the van't Hoff equation (Equation 3) was applied to help calculate temperature dependent logaO_2 values:

$$lnK_{eq} = -\frac{\Delta H°}{RT} + \frac{\Delta S°}{R} \quad (3)$$

where ΔH is reaction enthalpy at standard state, ΔS is entropy of the system at standard state, R= ideal gas constant, and T= temperature in Kelvin.

The presence of metal foils in the experiments buffers the solution at or below these lines, providing a highly reduced environment for Ni-NiO and Co-CoO, but a moderately reduced state for Cu-Cu_2O. The Ni-NiO and Co-CoO buffer lines are relatively close to the H_2O-H_2 (water stability) line compared to other buffer lines in Figure 1. Below the water stability line, hydrogen is being reduced from +1 to a zero-valence state, as seen below:

$$2H^+ (aq) + 2e^- \rightarrow H_2(g) \quad (4)$$

At temperatures where the stability lines for Ni-NiO and Co-CoO come near the stability line for H_2O-H_2, native Co and Ni foils have the reduction potential to provide an environment where water is reduced and hydrogen gas is stable. It is therefore possible for the formation of hydrogen gas to occur during the experiments with Co and Ni foils.

1.5. Geologic Context

A number of hydrothermal (as opposed to magmatic) deposit types such as U-Ni unconformity, “five element suite” polymetallic vein, red bed copper, and native copper deposits have significant amounts of metal-arsenide minerals (Table I). The most notable similarity between each deposit type is that during formation, an oxidized, acidic, saline, metal-rich fluid containing significant amounts of sulfur or arsenic eventually interacts with a reducing zone somewhere within the deposit, causing ore minerals to precipitate out of the fluid and into the host rock, thus creating the ore body. A generalized schematic shown in Figure 3 displays this interaction.

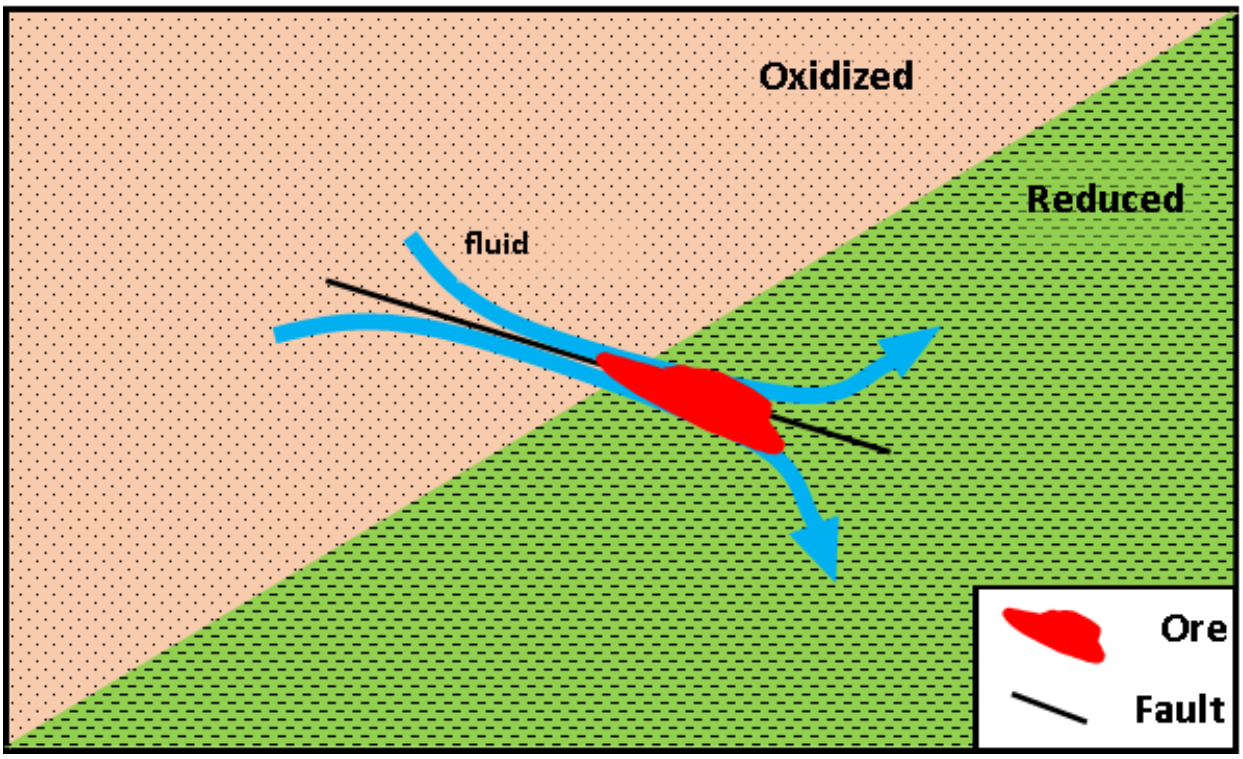

Figure 3. Simple schematic displaying the basic concept of ore formation by oxidized fluids interacting with a reduction front.

The abundance of metal-arsenide minerals in certain geologic environments is explained by the possibility that under the same conditions (temperature, pH, redox, solution composition, etc.), arsenite will be reduced at a faster rate than sulfate, consuming available dissolved metals and precipitating as solids.

2. Methods

2.1. Experimental Methods

2.1.1. Experimental Design

The experiments performed are separated into three experiment types: “separated”, or type A, “mixed”, or type B, and “mixed-timed”, or type C (Figure 4).

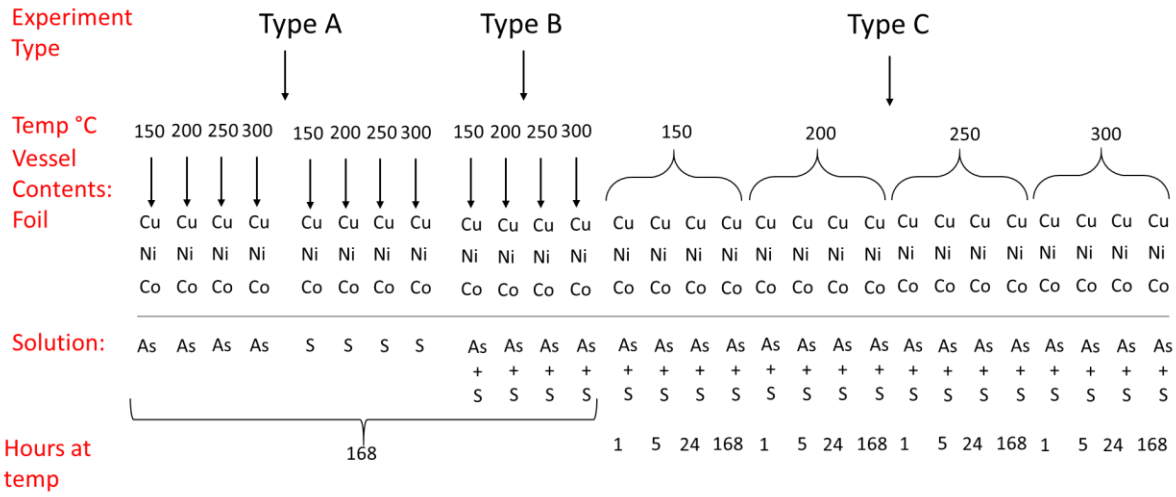

Figure 4. Experiment design matrix.

All three experiment types were similarly designed with a setup where synthetic hydrothermal fluids were interacted with a metallic foil in quartz-glass tubes (7mm ID, 9mm OD from Technical Glass) at elevated temperatures of 150°C -300°C in 50°C increments. This design allowed for possible thermochemical sulfate and arsenite reduction. For each experiment type, the variables were the duration of the experiment, the temperature, and the composition of the initial solution (Figure 4). The pressure was set to the liquid-vapor curve of water at the temperatures of the experiments.

The construction process of the glass tubes was similar to the methods in Gammons et al. (1997). Constrictions were created two thirds up the length of quartz glass tubes using a hydrogen-oxygen torch. Below this constriction, three to four milliliters (ml) of synthetic

hydrothermal solution were added. Above the constriction, an elemental foil 200 to 800 mg in size of either copper (Sigma-Aldrich, >99.99% pure, 0.125mm thick), nickel (Sigma-Aldrich, >99.99% pure, 0.125mm thick), or cobalt (Sigma-Aldrich, >99.9% pure, 0.25mm thick) was placed. The constriction allowed physical separation between the foil and solution until the experiment was ready to be conducted. Elemental foil was chosen because it acted as the primary reducing agent and as the source of metal cations for all the experiments performed. The sizes of the foils ensured that the concentrations of metal were high enough to potentially consume all the anions in solution through reduction reactions and to provide enough reducing capacity for the system. Before sealing the tubes, the insides of the tubes were placed under a partial vacuum of ≤ 0.67 atm using a hand pump.

The sealed silica-quartz glass tubes (typically about 15 cm in length) were placed three at a time into stainless-steel pressure vessels (Figure 5). A measure of 25 milliliters of water was added to the inside of the pressure vessels to equalize the pressure between the glass tubes and the pressure vessels, preventing the glass tubes from bursting at high temperatures. Because of this setup, pressures inside the glass tubes follow the liquid/vapor curve of water throughout the experiments.

A forced air convection oven (Thermo Scientific Heratherm or Fisher Scientific Isotemp) was used for temperature control. The autoclaves were placed into the oven upside down to equilibrate the solids with the solution at the set temperature (Figure 5). After a pre-determined period (Figure 4), the vessels were removed from the oven, re-inverted right-side up, and quenched in a vat of room temperature water (Figure 5). The re-inversion of the vessel was to separate the solution from the altered metal foil, ceasing further interaction. The operating procedure was similar for each experiment type.

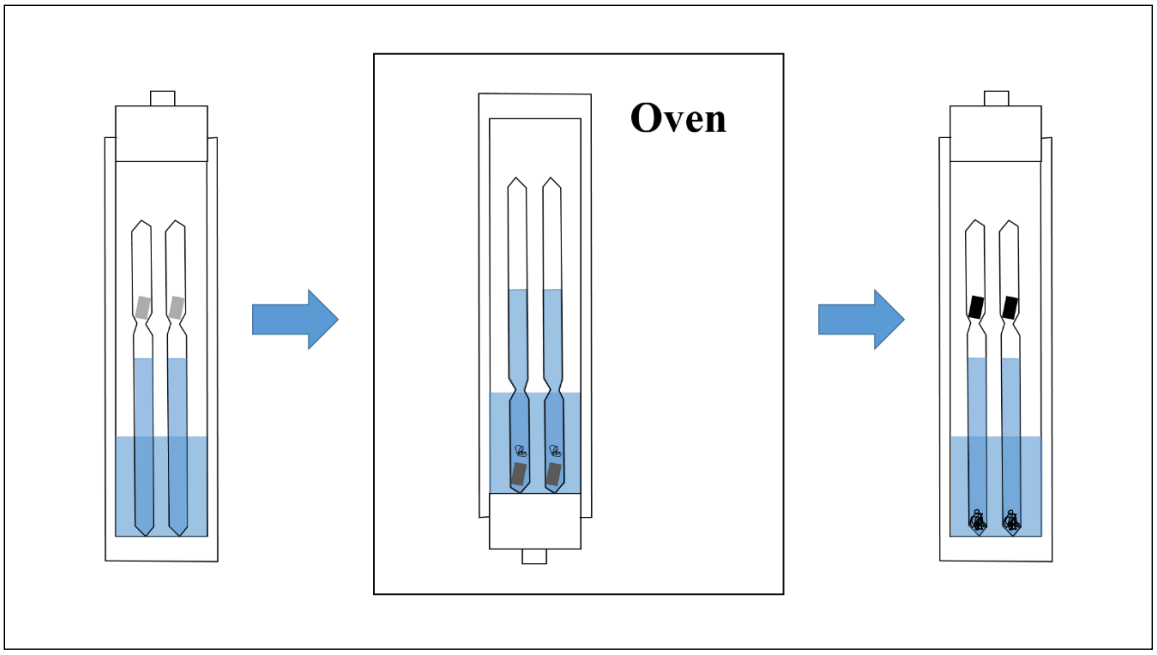

Figure 5. Schematic drawing of the basic premise of experimental methods. Sealed silica tubes were filled with a solution below the constriction and a foil perched above. The tubes and vessels were inverted while in the oven for up to a week. The vessels were then re-inverted and quenched.

The quick cooling of the solution inside the glass tubes during and after quenching can cause precipitates to form. Separating the foil from the solution right before quench allowed the quench products to form at the bottom of the tube, further separating the desired run products from the quench products. Sometimes, important precipitates can form at elevated temperatures and travel with the solution to the bottom of the tube upon inversion (e.g., Figure 11). These "run" precipitates are easily discerned from the quench products by plain observation (quench products forming while in the observer's line of sight several minutes after quench) or by their form/crystallinity (quench products are commonly fine-grained and subhedral to anhedral due to fast formation).

Upon quench, the silica tubes were removed from the pressure vessel and photographed for any ongoing reactions (Figure 6). The sealed tubes were massed before and after the experiment to test for leaks. After at least an hour (up to a day), the tubes were scored and

cracked open to extract the altered foils, precipitates, and post-experiment solutions to be analyzed. Extracted, altered foils were stored in the dry side of the cracked glass tubes. Solutions were stored either in a refrigerator in their glass tubes (wrapped with Parafilm) or in high density polyethylene (HDPE) Nalgene bottles.

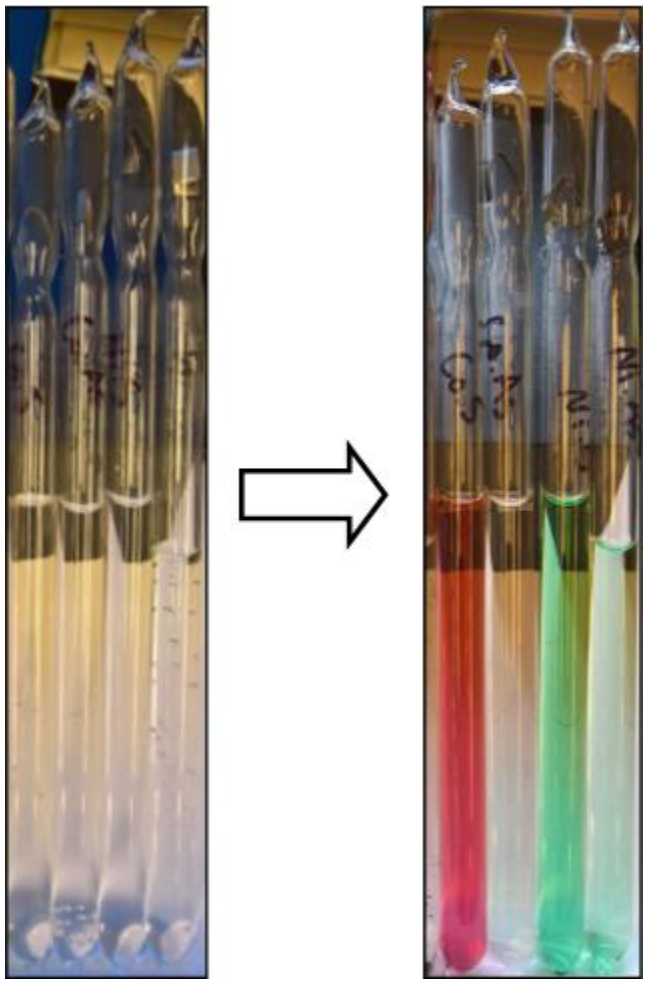

Figure 6. Photographs of Co-S, Co-As, Ni-S, and Ni-As tubes before (left) and after (right) an experiment run at 150°C.

2.1.1.1. Type A: Separated Solutions

The purpose of the preliminary experiments (type A) was to determine if sulfate or arsenite reduction could occur without catalysts within otherwise ideal conditions. A duration of one week was implemented to ensure evidence of TAR or TSR occurring.

Two different solutions were implemented for the type A experiments. One solution was a stock 1 N sulfuric acid, undiluted (FisherChemicals SA212-1). This concentration was chosen because it allowed for close to ideal solution conditions (high amounts of sulfate and a very low pH) to facilitate reduction. Thermochemical sulfate reduction within a reasonable timeframe without a catalyst at these experiment temperatures is notoriously difficult. An arsenite solution of stock 1000 ppm As(III) fixed in 2% hydrochloric acid (Sigma-Aldrich 72718) was used for the arsenite reduction experiment set. This solution was used for similar reasons as the sulfuric acid solution. Arsenite reduction reactions have not been widely studied, so a concentrated, acidic solution was used as a close imitation to natural hydrothermal systems where thermochemical arsenite reduction (TAR) might occur (Heinrich and Eadington, 1986).

In this experiment type, each individual tube contained a solution of either arsenite or sulfate and a foil of either Cu, Ni, or Co. The experiments were performed between 150°C - 300°C in 50°C ± 2°C increments, totaling twenty-four individual tubes (Figure 4). Each experiment was kept at elevated temperatures for one week.

2.1.1.2. Type B: Mixed Solutions

This experiment design was created to see if either sulfate or arsenite would preferentially reduce while in the presence of the other. Only one solution was used in this experiment set. The solution was an equal mix of 500 ppm H_2SO_4 and 500 ppm As(III) in 1% HCl. Although equal by volume, the solution has a molar ratio of 1.29, HSO_4^-:H_3AsO_3(aq). The

relative molar overabundance of sulfate was to compensate for the difficulty of reducing sulfate at ≤ 200°C in the type A experiment set, as seen in the results.

In this experiment type, each tube contained the solution mentioned above and a foil of either Cu, Ni, or Co. The experiments were performed from 150 to 300°C in 50°C ± 2°C increments, totaling twelve individual tubes (Figure 4). Each experiment was kept at elevated temperatures for one week or 168 hours. This was to ensure qualifiable evidence of TAR or TSR would be present.

2.1.1.3. Type C: Timed Mixed Solutions

After determining that sulfate and arsenite reduction occurred in the presence of each other (see section 3.2), the third experiment type was created to investigate whether there was a difference in the rate of the reactions occurring under the same conditions. The solution used in the type C experiments contained 500ppm H_2SO_4 and 500ppm AsO_2^- by dissolution of solid $NaAsO_2$ (Lab-Chem Cat# LC228709) in dilute sulfuric acid. This resulted in a solution with less acidity (pH ≈ 4) than the solutions used in the type A and type B experiments (pH < 2) because there was no hydrochloric acid to contribute to the acidity.

Four vessels with identical contents were put in the oven simultaneously and allowed to equilibrate with the set temperature. After the stable set-point was reached, one vessel was removed after one hour, the second after five hours, the third after twenty-four hours, and the fourth and final after one week (Figure 4). Any meaningful reactions in these sets of experiments are thought to occur either very quickly (within twenty-four hours) or slower (days to weeks), so time intervals on a log scale were implemented to accurately capture reaction progress (Figure 7).

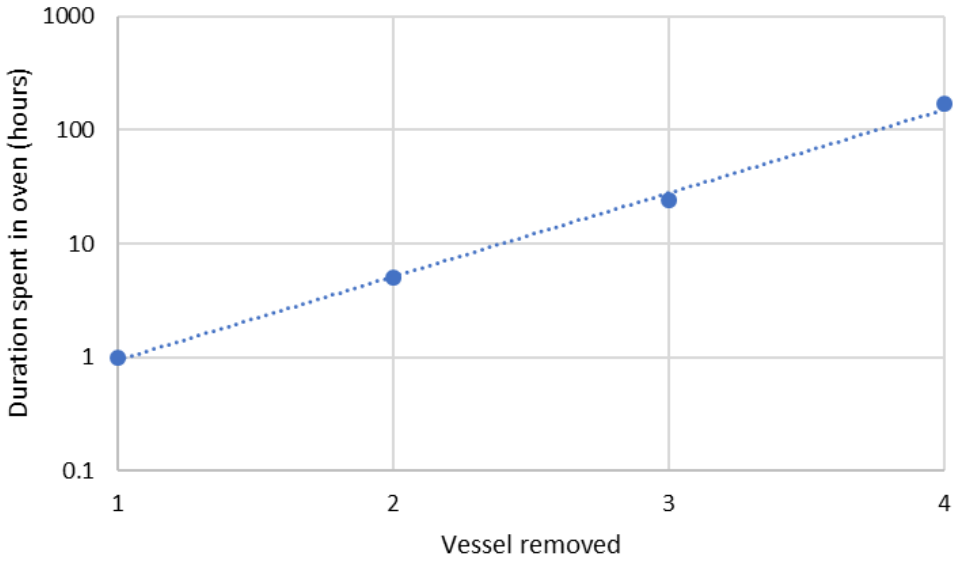

Figure 7. Duration of time that vessels 1 through 4 spent at an elevated temperature for a single type C experiment set. Notice the elapsed time is in log scale.

2.2. Analytical Methods

Solid products from the experiments were rinsed and dried at 40˚C before being examined by microRaman spectroscopy and scanning electron microscopy-energy dispersive x-ray spectrometry (SEM-EDS). Post experiment solutions were analyzed for concentrations of dissolved metals (copper, nickel and cobalt) and ligands (containing sulfate and arsenite) using an inductively coupled plasma mass spectrometer (ICP-MS) and an ion-exchange chromatography system (IC). An Ohaus Analytical Plus balance was used to weigh the foils, solutions, and sealed tubes for analytical calculations and identification post-experiment. A HACH spectrophotometer (DR 2010) was also used to perform bench-top measurements of concentrated sulfate solutions.

2.2.1. SEM-EDS

Chemical and textural analysis of the altered metal foils and precipitates was performed using a LEO 1430VP Scanning Electron Microscope (SEM) and an AMETEK EDAX Apollo 40

Energy Dispersive Spectrometer (EDS) with GENESIS XM4 LEO-32 V03.02.11 software at Montana Technological University. Backscatter imaging of the foils and precipitates produced the grayscale images in this paper. The relative abundances of elements in minerals formed on the altered foils and precipitates were determined by the EDS instrumentation on the SEM instrument. Atomic mass values and EDS spectra are reported for many of the analyses in Appendix A. Identification of specific mineral species in this paper was mainly performed by hand calculating the atomic mass values given by the EDS standard-less analysis to stoichiometric ratio equivalencies and by identifying physical characteristics of the minerals such as habit, crystal class/form, mineral association, and image greyscale brightness, which is proportional to average atomic mass.

To prepare for SEM analysis, samples were dried in a forced air convection oven at 60°C and placed on conductive graphite tape on round, stud-style, aluminum specimen mounts. The samples were then carbon coated (EMITECH K950X) to eliminate electron charging and distorted imaging. Therefore, carbon noted in the EDS spectra was disregarded.

2.2.2. MicroRaman Spectroscopy

The Renishaw inVia MicroRaman Spectrometer at Montana Technological University was used to produce Raman spectra of experimentally produced minerals and to create “true color” images using a reflected light microscope. The samples were placed on slides and analyzed with a 514 nanometer (nm) laser. The MicroRaman allowed for collection of detailed photographs of mineral samples, while simultaneously providing Raman spectra. These spectra were generally poorly expressed, as many of the minerals examined (sulfides, arsenides, alloys, and chlorides) do not have a strong Raman response, and reference spectra were not available for many minerals of interest.

2.2.3. Spectrophotometry

Bench-top measurements of aqueous sulfate were performed on highly concentrated samples using sulfate method 8051 on a HACH spectrophotometer. The data collected from this instrument were used to confirm correct solution concentrations of sulfate.

2.2.4. Inductively Coupled Plasma Mass Spectrometry (ICP-MS)

Post-experiment solutions were analyzed for metal concentrations using the ICP-MS located at the Montana Bureau of Mines and Geology (MBMG). Concentrated samples were diluted and acidified with 1% nitric acid to stabilize the solutions. Samples were analyzed following EPA Method 200.8 at the MBMG. Reported values were averaged from analysis of aliquots at 1x, 10x, and 100x sample dilutions.

2.2.5. Ion chromatography (IC)

Analysis of major anions by IC was performed at the MBMG following EPA Method 300.1. Concentrated samples were diluted to from 2 to 3 ml of sample solution to 25 ml of final solution to receive accurate readings.

2.2.6. pH readings

A Thermo Scientific Orion star AIII pH meter and a Hanna Instruments H1-1330 probe was used to determine the pH of stock and post-experiment solutions. The pH probe was fine enough that post-experiment solutions were left undisturbed and pH measurements were taken directly from the solutions in the silica tubing. When the H1-1330 probe was not available, an aliquot was removed and placed into an appropriately sized vial for proper measurement with another probe. The pH probes were calibrated using three standard buffer solutions of 2.00, 4.01 and 7.00 (Thermo Scientific Orion application solutions).

3. Results

3.1. Type A: Separated Experiments

In the type A experiments, the formation of arsenides and sulfides was abundant and obvious to both the naked eye and through SEM. TAR occurred at all temperatures for Cu, Ni and Co. TSR occurred at 250°C and 300°C for Cu, Ni, and Co.

3.1.1. Cu-S system

The Cu tubes containing the sulfate solution (Cu-S) produced the largest and most euhedral crystals of sulfides in this study. Chalcocite (Cu_2S) crystals formed freely in the solution producing needle-like and sawtooth-like morphologies (Figure 8) at 300°C and 250°C. Smaller hexagonal crystals of chalcocite also formed, with a distinct circular void piercing the center of each crystal. The Cu foil was consumed almost entirely by the formation of sulfide minerals, mainly chalcocite. There was also a change in color of the foil from pink (copper colored) to a matte black.

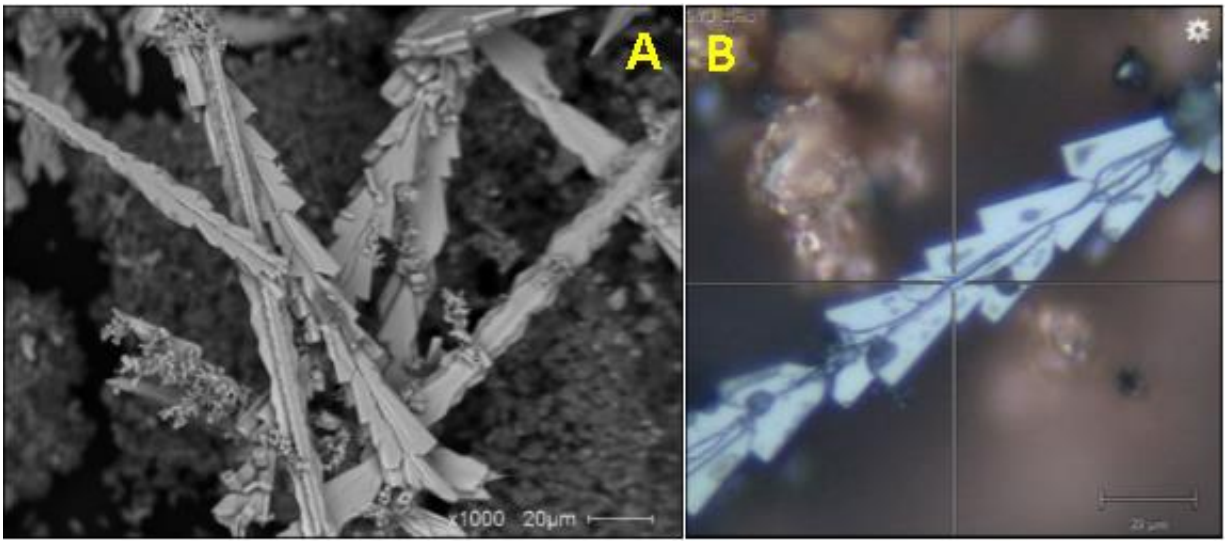

Figure 8. Needle-like chalcocite crystals produced in type A experiments (300°C, SEM image, A; 250°C, Raman micro photograph, B).
Other minerals and crystal forms seen in the Raman micrograph include native Cu (the dendritic, smaller crystals and background masses), Cu-sulfate minerals on quench, and hexagonal chalcocite crystals with voids in their centers.

Native Cu and Cu-sulfate precipitates formed on quench in these experiments, with greater amounts of these secondary precipitates forming from the lower temperature experiments where there was less sulfide production. Additionally, the color of some of the solutions changed from being colorless immediately after quench to a pale blue color several hours to days later. Both the color and the elemental Cu most likely formed by disproportionation of dissolved Cu(I) complexes upon cooling to room temperature. This reaction can be written as follows:

$$2Cu^{+}\,(aq) \rightarrow Cu^{2+}\,(aq) + Cu\,(s) \qquad (5)$$

At temperatures below 250°C, no copper sulfides formed. Foils were visibly tarnished but contained no sulfides; precipitates consisted entirely of native Cu crystals and hydrated Cu-sulfate phases. Solutions remained colorless in experiments where sulfides were formed.

3.1.2. Cu-As system

The Cu foils in the type A Cu-As experiments were entirely converted to Cu_3As at all temperatures tested. The altered foil was thin, light grey, and brittle with significant void space between each side, allowing the formation of an inner envelope of alteration minerals (Figure 9). The produced minerals consisted almost entirely of domeykite (Cu_3As, Figure 10 panel D), with the scattered formation of nantokite (CuCl) crystals with maximum widths of ~10 micrometers (μm). Formation of domeykite could occur by the following reaction:

$$H_3AsO_3\,(aq) + 6Cu\,(s) + 3H^{+}\,(aq) \rightarrow Cu_3As\,(aq) + 3Cu^{+}\,(aq) + 3H_2O\,(l) \qquad (6)$$

The precipitate that formed upon quench consisted of almost entirely nantokite. Some nantokite crystals (Figure 10) were as long as 1mm before the extraction of the crystals broke them. The nantokite crystals came out of the pressure vessels white, but over the course of two to eight hours, exposure to light changed their color to a blue hue. The coloration darkened as exposure to light persisted (Figure 11).

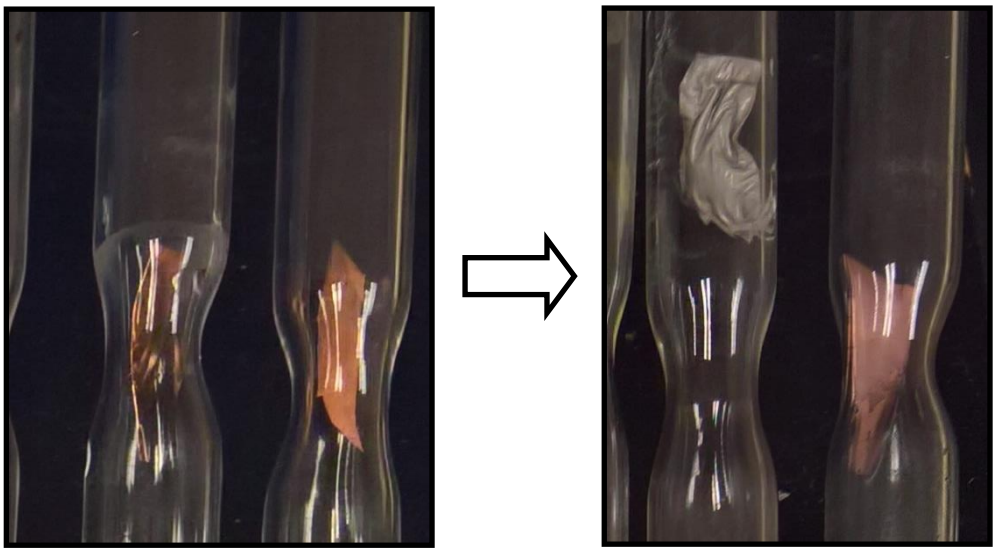

Figure 9. Changes in Cu foils between the beginning and end of the 250°C type A experiment.
A Cu-As tube (left tube in both pictures) and a Cu-S tube (right tube in both pictures) before (left pane) and after (right pane) an experiment run at 250°C. Foils were approximately 1 cm in length at their longest axis.

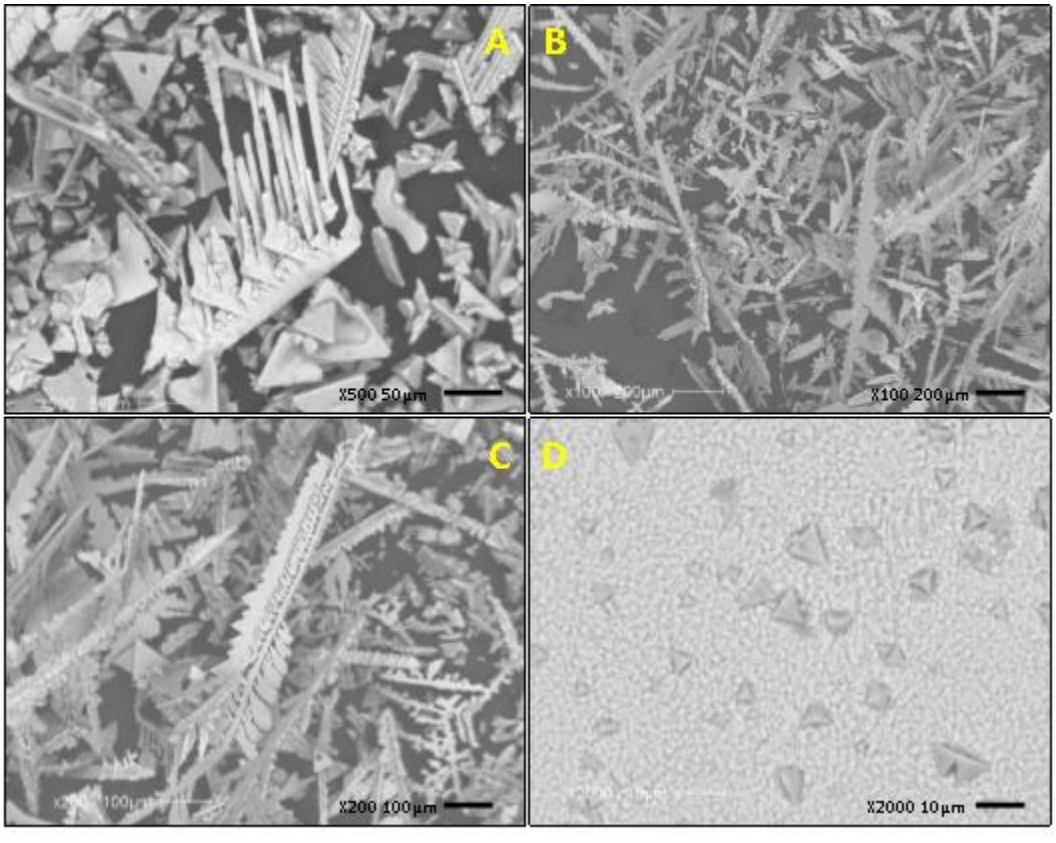

Figure 10. Different morphologies of CuCl found in type A Cu-As experiments.
Panel A: 300°C type A experiment; bladed, stringer, and pyramid morphologies are present. Panels B, C, and D: 150°C type A experiments (As only); bladed, branching shapes and CuCl pyramids on domeykite foil (D).

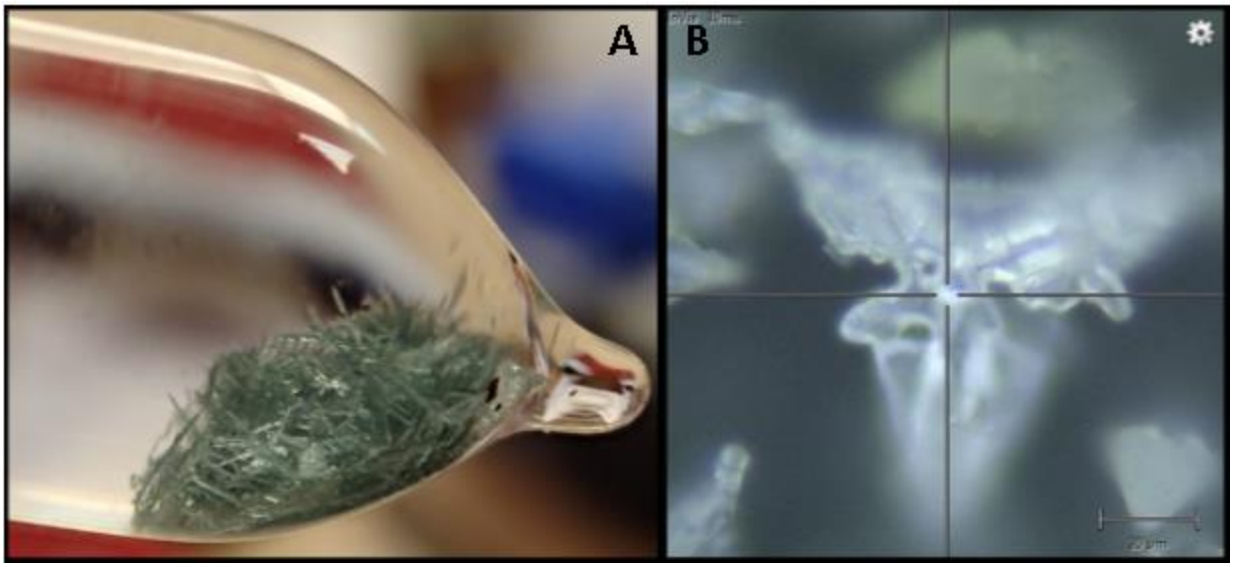

Figure 11. CuCl crystals formed from a type A Cu-As experiment at 300°C.
CuCl crystals after 1-2 hours of light exposure; silica tube (9mm OD) for scale (A) and an individual CuCl crystal photographed in reflected light (B).

The mineralogy of the secondary precipitates differed in the Cu-S system and the Cu-As system. In the former, SO_4^{2-} was the dominant ligand, whereas in the latter, both arsenite (H_3AsO_3,aq) and chloride (Cl^-) were prominent. The presence of high Cl^- concentration in the Cu-As system stabilized the cuprous ions upon quench as dissolved Cu(I) chloride complexes (Xiao et al., 1998). For this reason, the dissolved Cu(I) did not disproportionate on quench in the Cu-As experiments, and no elemental Cu was seen in the precipitates at the bottom of the tubes. Instead, the excess dissolved Cu(I) precipitated as CuCl (s).

3.1.3. Ni-S system

TSR occured within the Ni system only at 300°C. Ni-sulfides mainly identified as vaesite (NiS_2) were formed as a precipitate found at the bottom of the tube (Figure 12) and coating the foil. The vaesite crystals that formed were euhedral with a cubic habit (Figure 12). The foil was heavily tarnished to a dark shade of grey and was thickly coated with green Ni-

sulfate ($NiSO_4 \cdot 6H_2O$). These textures suggest that the Ni-sulfate coatings formed quickly during this experiment by a reaction such as:

$$Ni\,(s) + SO_4^{2-}\,(aq) + 2H^+\,(aq) \rightarrow NiSO_4\,(s) + H_2\,(g) \quad (7)$$

Reduction of SO_4^{2-} to H_2S must have been slower, inferred by crystal habit. This could involve $H_2(g)$ being liberated by reaction (7):

$$SO_4^{2-}\,(aq) + 4H_2\,(g) + 2H^+ \rightarrow H_2S\,(g) + 4H_2O\,(l) \quad (8)$$

The H_2S then reacted with $NiSO_4$ to form NiS_2, as seen below:

$$NiSO_4 + 2H_2S \rightarrow NiS_2 + SO_4^{2-} + 2H^+ + H_2(g) \quad (9)$$

In this reaction, sulfate is reduced to polysulfide S_2^{2-}, as the valence of sulfur in NiS_2 is -1, as is the case for pyrite (FeS_2). Because the Ni foils were already coated by Ni-sulfate, the NiS_2 precipitated directly from solution and fell to the bottom of the tubes on quench.

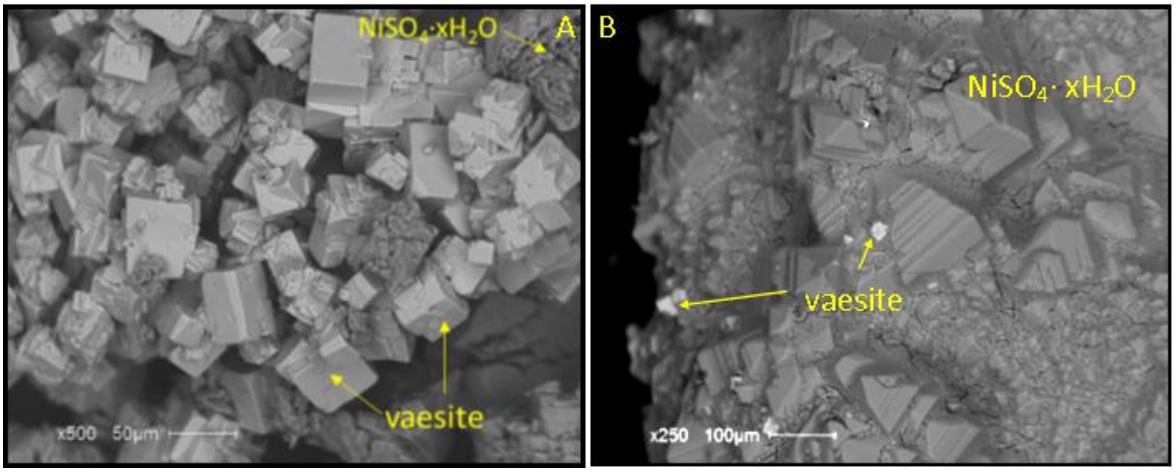

Figure 12. SEM images of vaesite (NiS_2) precipitate formed at 300°C accompanied by Ni-sulfates. Notice the complex crystallinity of the Ni-sulfates.

At temperatures below 300°C, no noticeable Ni-sulfides were formed. The lack of sulfides was accompanied by a green-colored solution, evidence of highly concentrated Ni^{2+} (Figure 6). The Ni^{2+} in solution is thought to be dissolved nickel from the oxidation of the Ni foil to Ni^{2+}, but without appropriate conditions for the dissolved Ni^{2+} to precipitate. The fact that Ni-

sulfate solids were abundant in the 300˚C experiment but not at lower temperature is consistent with the idea that the solubility of solid Ni-sulfate is probably retrograde, by analogy to other sulfate minerals such as anhydrite (Holland and Malinin, 1979).

The 150°C tube exploded violently upon opening. This could be because of the production of hydrogen gas (Equation 7). At 150°C, the dissolution of nickel may produce hydrogen gas but this gas which is normally consumed by the reduction of sulfate (Equation 8) builds up, as TSR cannot occur at such low temperatures. This would allow for a positive pressure condition inside the glass tube and enable it to erupt violently upon opening.

3.1.4. Ni-As system

Ni foils at all temperatures tested produced a flaky skin of an unidentified Ni-arsenide, either Ni_3As or Ni_5As_2 (Figure 13) around the entire foil. This could have occurred similarly to the reactions for the formation of nickeline (NiAs) and rammelsbergite ($NiAs_2$) below:

$$2H_3AsO_3\ (aq) + 5Ni\ (s) + 6H^+\ (aq) \rightarrow 2NiAs\ (s) + 3Ni^{2+}\ (aq) + 6H_2O\ (l) \quad (10)$$

$$2H_3AsO_3\ (aq) + 4Ni\ (s) + 6H^+\ (aq) \rightarrow NiAs_2\ (s) + 3Ni^{2+}\ (aq) + 6H_2O\ (l) \quad (11)$$

The foils had to be scraped gently to expose the Ni foil underneath. Figure 13 shows dendritic crystals of Ni_5As_2 as overgrowth on a massive, botryoidal rind of $Ni_xAs_yCl_z$. At lower temperatures such as at 150°C, the flaky rind was entirely $Ni_xAs_yCl_z$. The habit of the Ni_5As_2 became more anhedral at lower temperatures, until the formation of Ni_5As_2 ceased at 150°C. Ni_5As_2 has been reported in some publications for the Bon Accord deposit in South Africa as $Ni_5(As,Sb)_2$ (Tredoux et al., 2016), but it is not listed as a known mineral. Solution color intensity varied a little at the different temperatures, with more intense green hues at lower temperatures (Figure 6). The 150°C tube burst, but less violently than the Ni-S tube mentioned previously.

Figure 13. Ni_5As_2 and $Ni_xAs_yCl_z$ formed on a Ni foil at 150°C.

3.1.5. Co-S system

Due to the production of an odorless gas, the 300°C run exploded in the pressure vessel, with repeatable results. At 150°C, the tube was under positive pressure, noted by a small "pop" when scored, but the tube did not erupt violently. No precipitates were formed at any temperature, and the aqueous solution took on a deep pink color, indicative of dissolved cobalt (Co^{2+}), at lower temperatures (150°C and 200°C; see Figure 6). All foils appeared nearly identical before and after the experiment, except when a very small amount of foil was used for a 300°C run and the foil dissolved completely.

3.1.6. Co-As system

The 300°C tube in this experiment burst upon scoring. This caused most of foil to be lost, but fortunately a portion of foil fell into the solution during the explosion and was recovered for SEM analysis. SEM analysis showed that cobalt arsenide minerals, possibly safflorite ($CoAs_2$), replaced the foil entirely at 300°C. This could occur as described below:

$$2H_3AsO_3\ (aq) + 4Co\ (s) + 6H^+\ (aq) \rightarrow CoAs_2\ (s) + 3Co^{2+}\ (aq) + 6H_2O\ (l) \qquad (12)$$

Precipitated $CoCl_2$ salt was also present as a very thin crust on a small portion of the foil analyzed. At lower temperatures, such as at 150°C, the foil was corroded and displayed large amounts of some unidentified Co-arsenide. This Co-As phase can be either interpreted as an arsenide mineral, or perhaps as an alloying of elemental Co and As, as there was no distinct growth of a new mineral on the surface of the foil but instead intense corrosion around the edges of the foil. Along the edges, at least three different Co-As solid phases were present with at least one being an alloy (Figure 14). Spatial relationships between the different compounds appeared random and messy. These species have stoichiometric relationships not known to natural minerals (Co:As ratios of 10:1, 20:1). The pure cobalt rich end-member minerals of langisite ((Co,Ni)As) or modderite ((Fe,Co)As) may have formed (Figure 14). The solution was relatively clear with only a slight pink coloration, unlike the Co-S experiment.

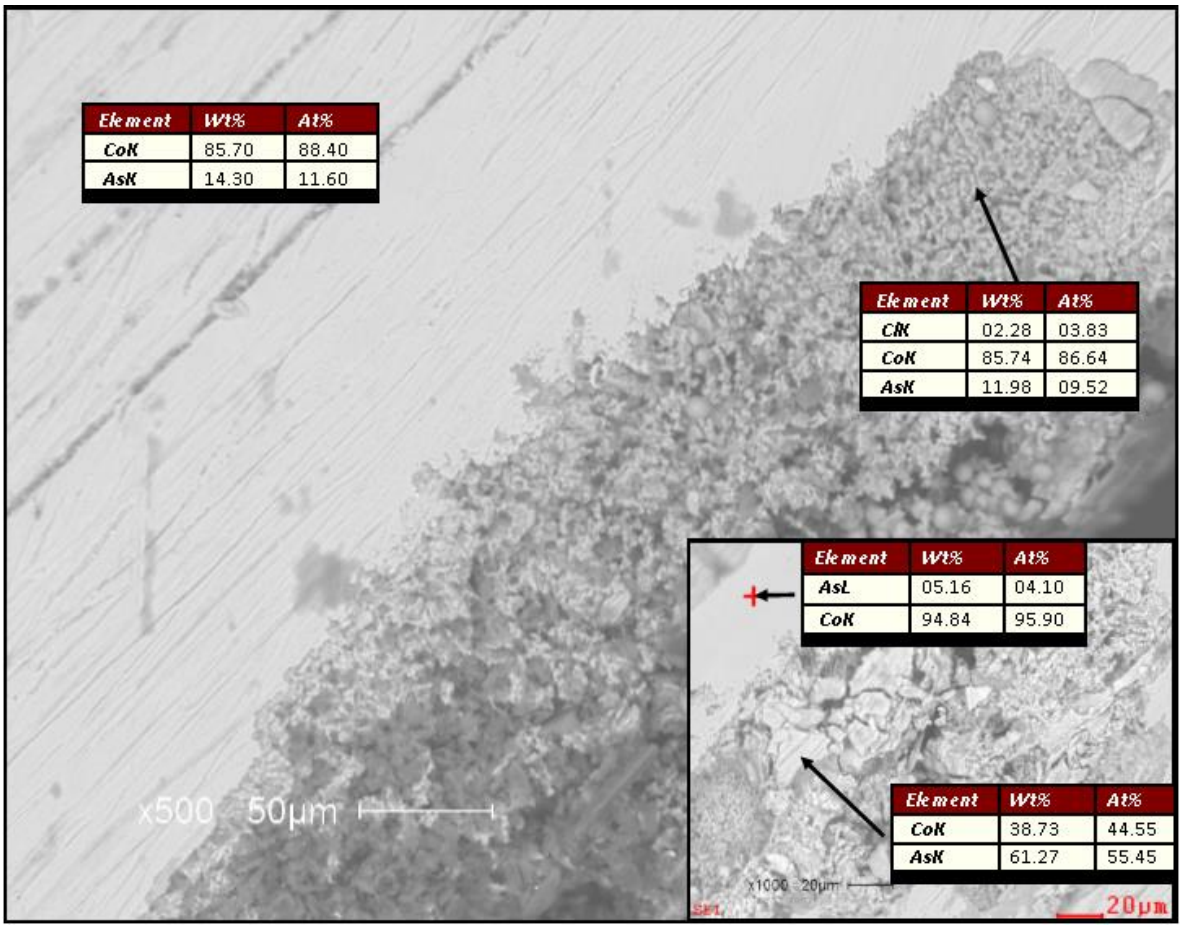

Figure 14. SEM images of a Co-As foil altered at 150°C displaying multiple phases of Co-As (Co-arsenides or a Co-As alloy).

3.2. Type B: mixed experiments

The type B experiment set produced some of the most interesting results in this study and exhibits a strong parallel with the type A experiment set: arsenide minerals and sulfide minerals formed, but sulfide minerals only formed at temperatures at or above 250°C. Due to the nature of the experiment, this means that some tubes contained both sulfide minerals and arsenide minerals and even sulfarsenide minerals. The co-existence of both arsenide minerals and sulfide minerals results in textural relationships between the two (or more) phases that could help this study further understand TSR and TAR reaction rates.

3.2.1. Cu-As-S system

At temperatures of 250°C or above, the Cu foil was altered to Cu-arsenide minerals with subsequent Cu-sulfide crystal growth (Figure 15A). Below 250°C, only Cu-arsenide minerals were present (Figure 15B). Both domeykite and Cu_5As_2 were identified as minerals replacing the foil. The Cu-arsenide minerals appear to have anhedral forms as seen at the resolution of the SEM.

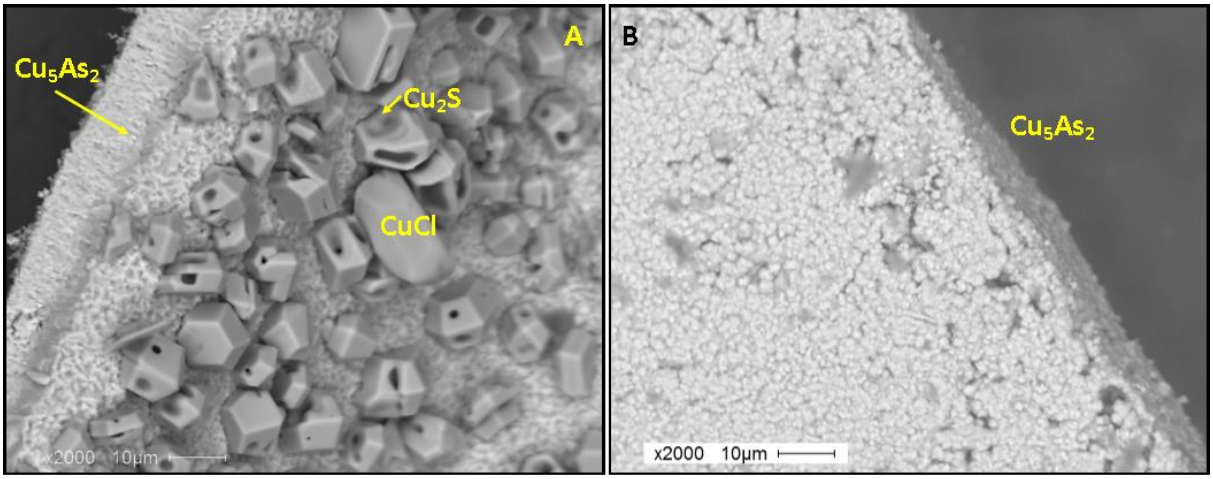

Figure 15. SEM images of foils from the Cu-As-S system at 300°C (A) and 150°C (B).

The only sulfide mineral species formed in the type B experiments was chalcocite at 250°C and 300°C. The chalcocite was euhedral (average crystal sizes of 8-10 µm across the longest axis), clearly demonstrating its hexagonal morphology in the form of hexagonal bifrustums (Figure 15A), identified by twelve trapezoidal faces with two additional hexagonal faces. On most of these crystals, there were holes perforating the center of the faces, which could be because of "hopper" crystal type growth or as etch pitting. This could indicate disequilibrium of chalcocite at some point in time after formation or under-saturation of the solution at the very end of the experiment, perhaps even during/after quench. Another idea for the perforated, "hopper" style crystallization is that the chalcocite crystals grew around already

existing CuCl crystals. The CuCl crystals could have then dissolved sometime after chalcocite overgrowth. This would result in a skeletal habit, with somewhat hollow chalcocite crystals.

The anhedral arsenide mineral matrix indicates quick replacement reactions (equation 6) occurring at the onset of the experiment. The larger, euhedral, chalcocite crystals appear to have subsequently grown on top of the arsenide mineral matrix.

3.2.2. Ni-As-S system

In the Ni-As-S type B experiments, both Ni-sulfide minerals and Ni-arsenide solids formed at 300°C, like the Ni-S and Ni-As systems in the type A experiments. Like the Cu-As-S system, the texture of the foil/crusts show an arsenide substrate on which Ni-sulfide minerals then grew (Figure 16).

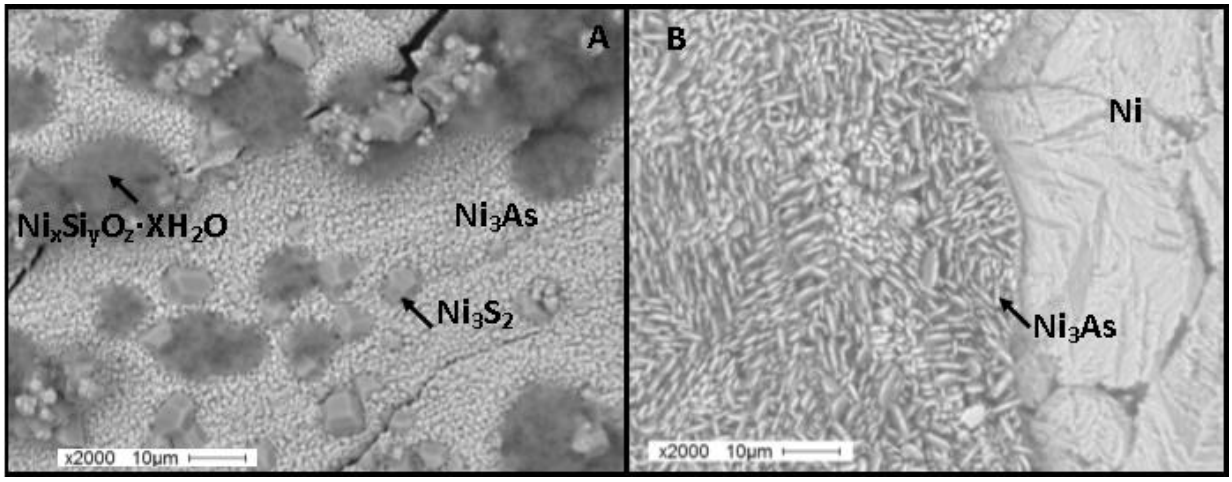

Figure 16. SEM images of foils from the Ni-As-S system at 300°C (A) and 150°C (B).

The Ni-arsenide solids appeared fine-grained and massive to botryoidal, while the sulfide minerals had a more distinct crystal shape (Figure 16A). The Ni-sulfide crystals were identified as heazlewoodite (Ni_3S_2), and the Ni-arsenide solids were identified as Ni_3As (Figure 16). Ni_3As is not a recognized mineral, but it is listed as an unnamed Ni-arsenide mineral from the Bon Accord deposit, S Africa (Tredoux et al., 2016).

At temperatures below 250°C, no sulfide minerals were formed. This paralleled the Cu-As-S system. Interestingly, lower temperature formation of Ni-arsenide solids produced euhedral crystals, with crystals forming complex hexagonal plates with a somewhat ordered habit as a crust on top of the remnant nickel foil (Figure 16B).

3.2.3. Co-As-S system

Like the previous systems within the type B experiments, this system produced Co-sulfide minerals and Co-arsenide minerals at 300°C. The textures were like the other systems in that metal-sulfide minerals grew upon a metal-arsenic substrate, but the substrate in this system consisted of a Co-sulfarsenide mineral (cobaltite, CoAsS; Figure 17) instead of metal-arsenide solids as seen previously (Figures 15 and 16). The largest crystals of Co-sulfide minerals at 300°C had widths of 5-6 µm, with most of the crystals being 2-3 µm across.

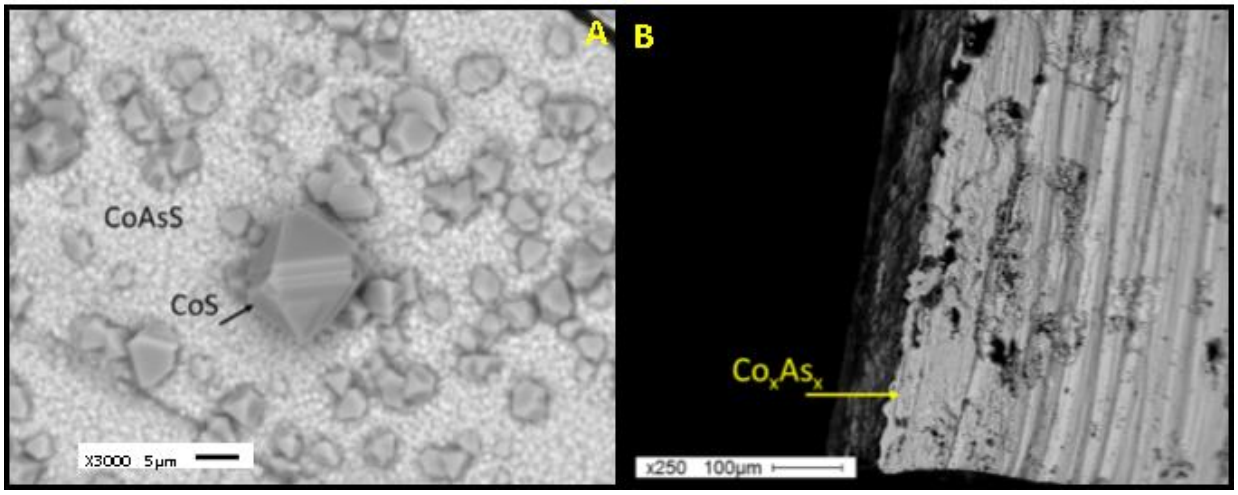

Figure 17. SEM images of altered foils from the Co-As-S system at 300°C (left) and 150°C (right). CoS crystals were euhedral with some complicated structuring.

Figure 17 also revealed interesting mineral grains which had clear staggered growth and were large compared to other crystals that formed. This mineral was identified as CoS (jaipurite)

based off its habit and EDS signature. The jaipurite grew similarly to the previous type B experiments: as crystals on-top of an anhedral matrix, and, in this case, a matrix of cobaltite.

The metallic foils in the Co-As-S system were the least altered foils throughout this experiment set. The foils retained most of their mass (>95%) as pure Co and had the thinnest apparent alteration layers/crusts of the metallic foils tested. Many of the Co-foils had crusts that, when handled or cut, rubbed off quite easily like a tarnish and did not flake like other foils, especially the Ni-foils.

Stoichiometry for certain Co_xAs_x compounds, especially foils reacted at lower temperatures (in atomic %: Co, 95.7%; As, 4.3%), suggest arsenic integration into the Co metal; perhaps as a thin, low proportion Co-As alloy. When edges of the Co-foils were measured, readings indicated a pure core. The thick, rectangular, wire like shape of the Co foil could have contributed to such a diverse reaction gradient.

3.3. Type C: mixed timed experiments

The type C experiment set was not as successful as type A or type B experiments in consistently producing sulfide minerals or arsenide minerals. Abundant oxides such as cuprite (Cu_2O), Ni-oxides, and Co-oxides and sulfates (like Ni-sulfates, Section 3.1.3) were observed under SEM as crystals or crusts eroding the otherwise untouched metal foils at nearly all temperatures.

3.3.1. Cu-As-S system

No apparent sulfide minerals or arsenide minerals were formed during the Cu-As-S type C experiments. Metal foils appeared slightly tarnished to the naked eye. There was slight discoloration from the earlier vessel to the latest vessel, although there was little change in the severity of tarnishing. Under SEM, the foils had pitting with anhedral to euhedral cuprite (Cu_2O)

crystals residing within pits at ~8-10 µm across along their longest axis (Figure 18). The severity of pitting and size of Cu-oxide crystals changed slightly across temperature and time. At 300°C, euhedral oxide crystal formation started almost immediately, with pitting and crystals seen in the first hour. These crystals then grew larger as time increased. At lower temperatures, an oxide crust appeared first, which then dissipated to larger, fewer euhedral oxide crystals (60 µm along longest axis) in pits, with elapsed time (Figure 19).

In the Cu-As-S type C experiments, the complete lack of sulfides and arsenides present is a stark contrast to type A and type B experimental results discussed so far. Again, this may be a product of a higher pH due to the lack of hydrochloric acid in the starting solution, putting the experimental conditions into a different Eh-pH regime.

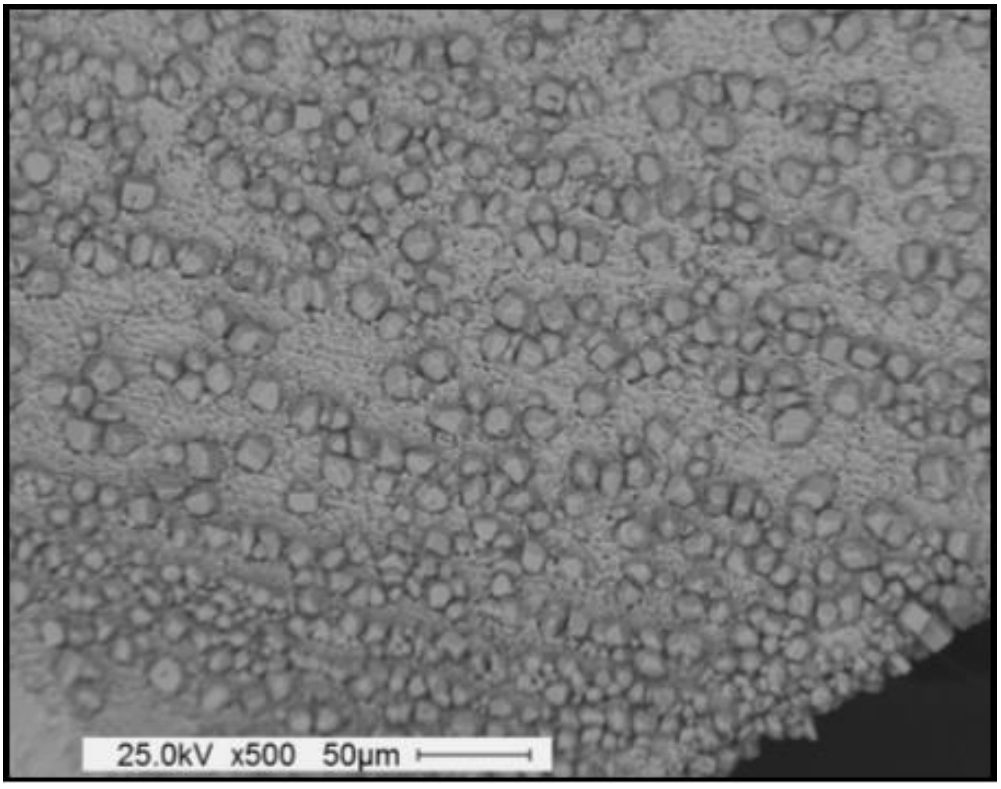

Figure 18. SEM image of a Cu foil pitted with cuprite that reacted for one hour at 300°C. The matrix texture appeared to be etched Cu-foil, revealing the crystal boundaries between natural crystals within the metallic foil.

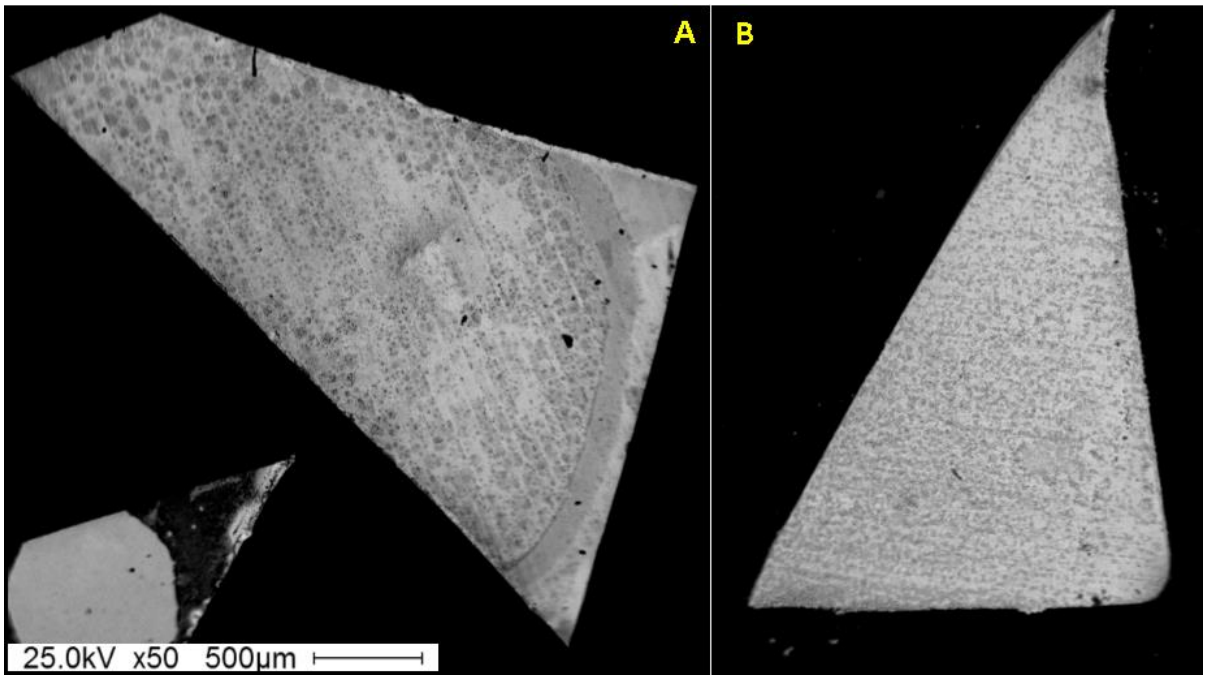

Figure 19. Two copper foils at 150°C after reacting for one hour (A) and for a whole week (B).

3.3.2. Ni-As-S system

Arsenide minerals and sulfide minerals formed sporadically throughout the Ni-As-S type C experiments, with no direct trend (Figure 20). The formation of Ni_3As_2 was seen only in samples from higher temperature experiments (300°C and 250°C), and the Ni_3As_2 was only present as a very thin layer between Ni-sulfates and suspected Ni-arsenates. EDS spectra for many of the phases including Ni, As, or S indicated the presence of oxygen in nearly every analysis, ranging from 1-23 atomic % oxygen. Because of this, arsenide mineral or sulfide mineral presence was unlikely with only two analyses confirming otherwise (see Appendix A). Products formed from the experiment did not appear to vary with time, and crust thickness did not change to a notable degree. Crystal size of the sulfate minerals and arsenite minerals did seem to change, with crystals being larger at longer time intervals.

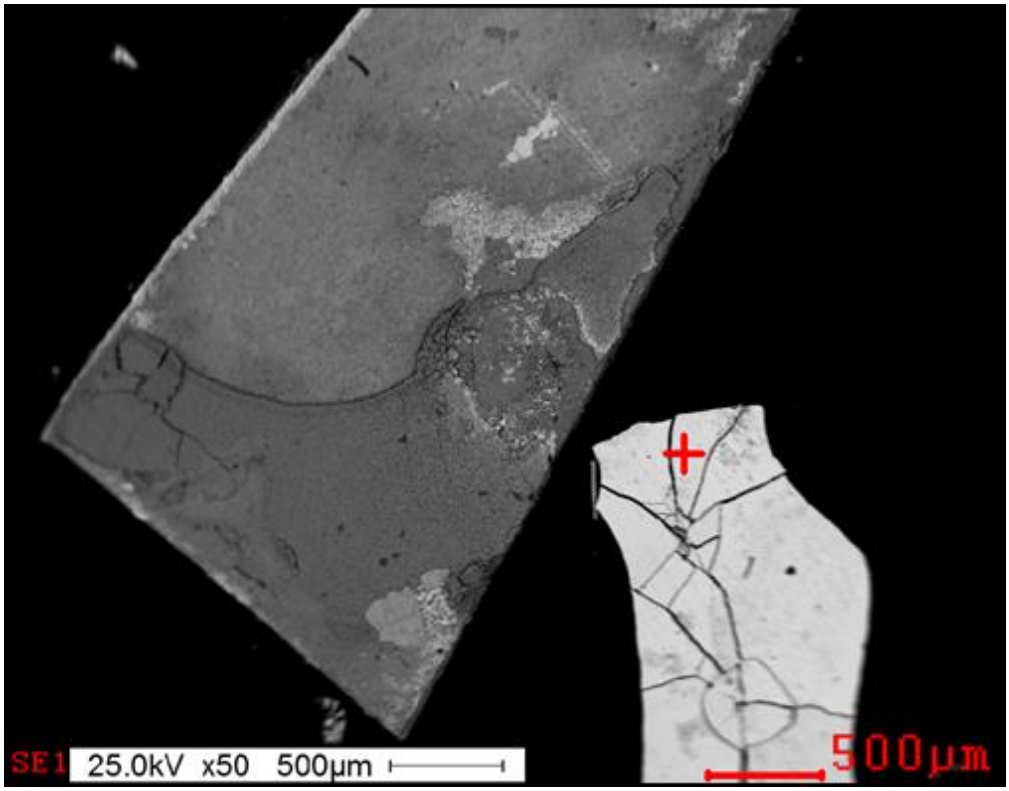

Figure 20. Ni foil after one week at 250°C.
Layered alteration crusts formed, with certain layers being a nickel arsenide (white left).

3.3.3. Co-As-S system

Limited amounts of arsenide and sulfide minerals formed in the Co-As-S type C experiments. Mineral formation was mainly seen as crusts and shallow rinds on the Co foil surface (Figure 21). Some Co-As alloying as seen on other Co foil results (Section 3.2.3) also occurred here. One spot of pure Co-langisite ((Co,Ni)As) was observed at 300°C (Figure 21), but otherwise mineralization was sporadic and limited.

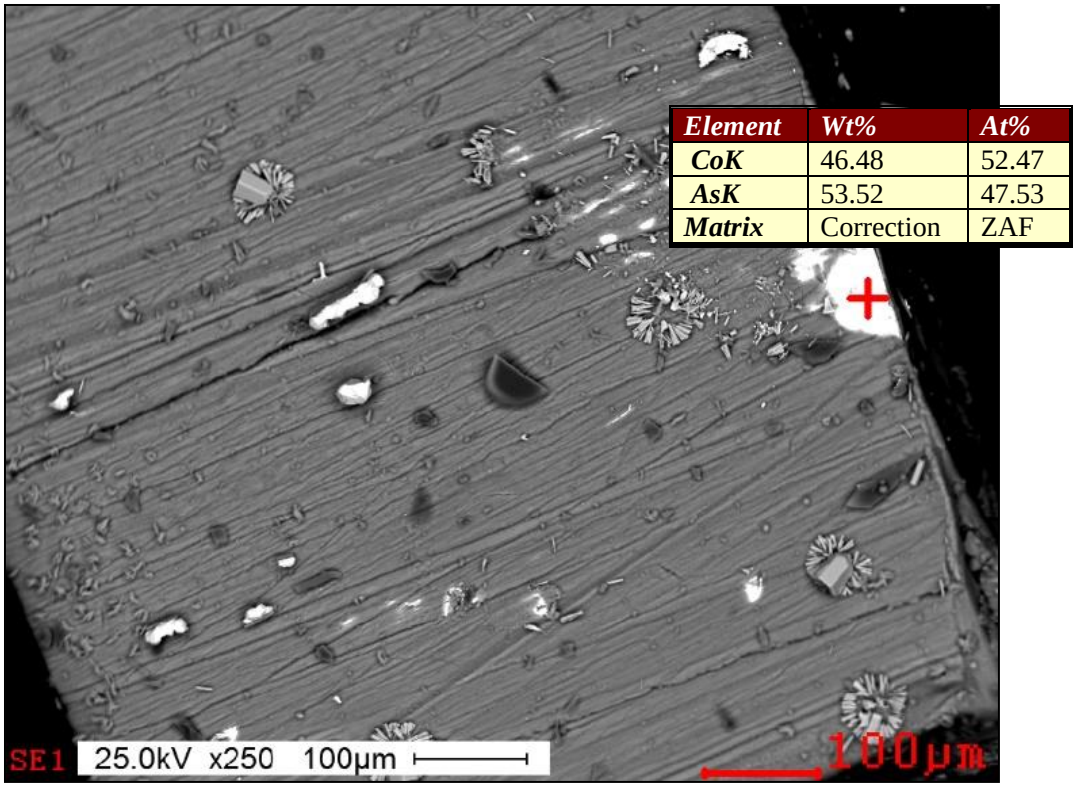

Figure 21. SEM image of a Co foil after one week at 300°C displaying few euhedral crystals. Bright spot highlighted by the crosshairs is a spot of CoAs, or langisite (usually described as (Co,Ni)As).

Co-arsenite minerals had euhedral crystals and were complex (Figure 22). These minerals were not observed to be products of either TAR or TSR, but instead seemed to be minerals formed upon quench that contained the still oxidized sulfate or arsenite, with SiO_2 contamination from the glass tubes. The mineral "splinters" surrounding the larger euhedral mineral appeared to be of the same composition. The euhedral Co-arsenite mineral or Co-arsenate-sulfate mineral had an elongated hexagonal form (Figure 22). There were visible growth striations along the a and b axes of the mineral, which terminated with a concave, dish like appearance on one end (see shadow in Figure 23). The other terminus (in contact with the foil crust) appeared to end in a crude point (Figure 23).

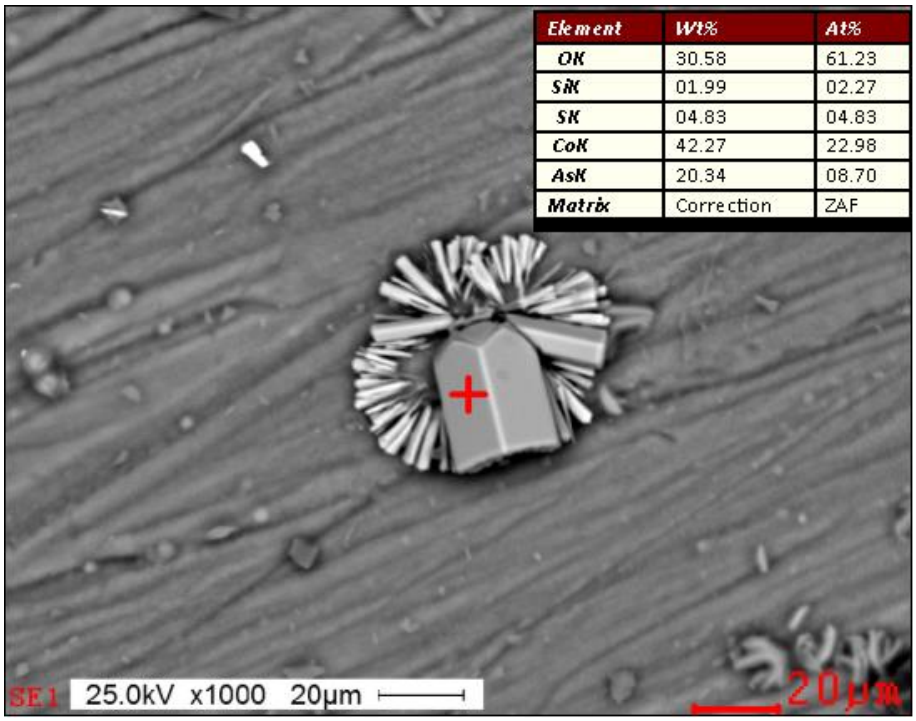

Figure 22. Co type C experiment at 300°C showing euhedral crystals of possibly Co-arsenite. The SEM analysis is of the spot indicated by the red crosshairs.

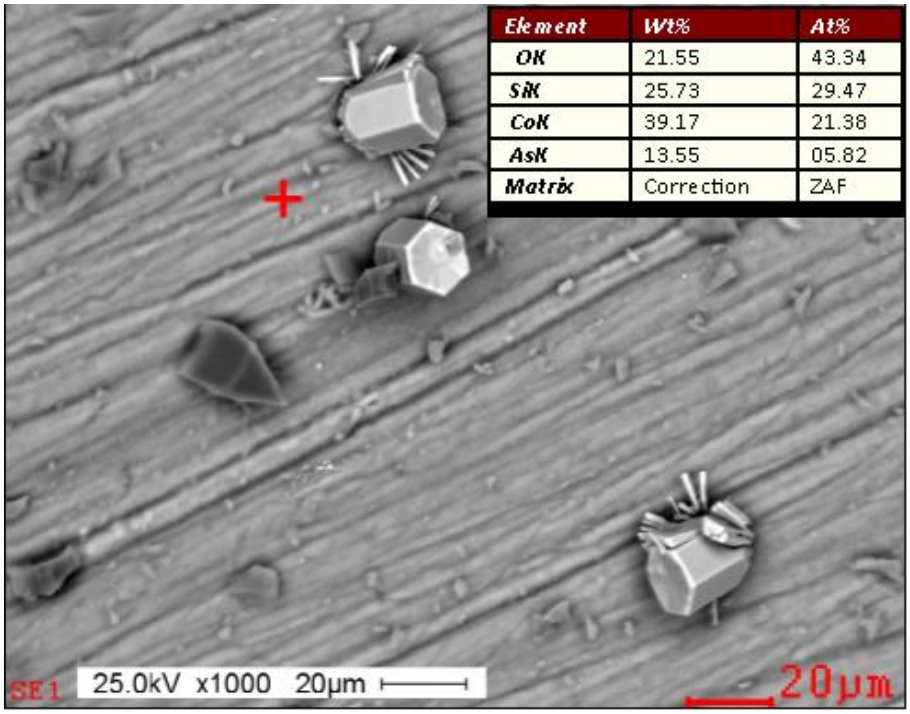

Figure 23. SEM image showing the barrel shaped, hexagonal Co-arsenite with growth striations. The bottom-most barrel shows clean fractures, indicating a possible cleavage plane. The darker angular shapes are silica glass from the removal process.

The darker background in Figures 22 and 23 was not pure Co foil, but instead an amorphous crust of a complex Co-As silicate mineral. The smaller, lightly shaded angular mineral grains present were difficult to analyze with the SEM-EDS due to their size and because they seemed to be imbedded into the alteration rind. It is unknown if these grains are important to the TAR process. At lower temperatures, some specks of Co-As-silicate were present, but were not as well formed and were much smaller (>10 μm). The rinds appeared to be more delicate and thinner on the foil surface. No other minerals were apparent.

4. Discussion

4.1. Experimental Results

Results from the type A, B, and C experiments are summarized in Tables II and III. The results show that thermochemical arsenite reduction occurred (1) at lower temperatures and (2) at a faster rate than thermochemical sulfate reduction. A summary of run products performed at different temperatures and solution conditions (Figure 24) confirms this statement. Both TAR and TSR reactions took place in the type A and B experiments at 250 and 300°C, but at 150 and 200°C, only TAR occurred. In addition, in the 250 and 300°C experiments, the textures of the foils suggest that TAR occurred quickly, resulting in complete transformation of elemental foil to metal-arsenides or sulf-arsenides, whereas TSR occurred slowly, allowing larger metal-sulfide grains to form on top of the finer-grained arsenide minerals.

Table II. Summarized results for type A and type B experiments.
Experiment results with "?" indicate questionable evidence and deserve further investigation.

	Type A			Type B		
Temp °C	Cu	Ni	Co	Cu	Ni	Co
150	TAR	TAR	TAR?	TAR	TAR	TAR?
200	TAR	TAR	TAR?	TAR	TAR	TAR?
250	TAR/TSR	TAR	TAR?	TAR/TSR	TAR/TSR	TAR
300	TAR/TSR	TAR/TSR	TAR	TAR/TSR	TAR/TSR	TAR/TSR

Table III. Summarized results for type C experiments.

Type C												
	150°C			200°C			250°C			300°C		
Time (hrs)	**Cu**	**Ni**	**Co**	**Cu**	**Ni**	**Co**	**Cu**	**Ni**	**Co**	**Cu**	**Ni**	**Co**
1	-	-	-	-	-	-	-	-	-	-	-	-
5	-	-	-	-	-	-	-	-	-	-	-	-
24	-	-	-	-	-	-	-	TAR	-	-	TAR	TAR?
1 week	-	-	-	-	-	-	-	TAR	-	-	TAR	TAR

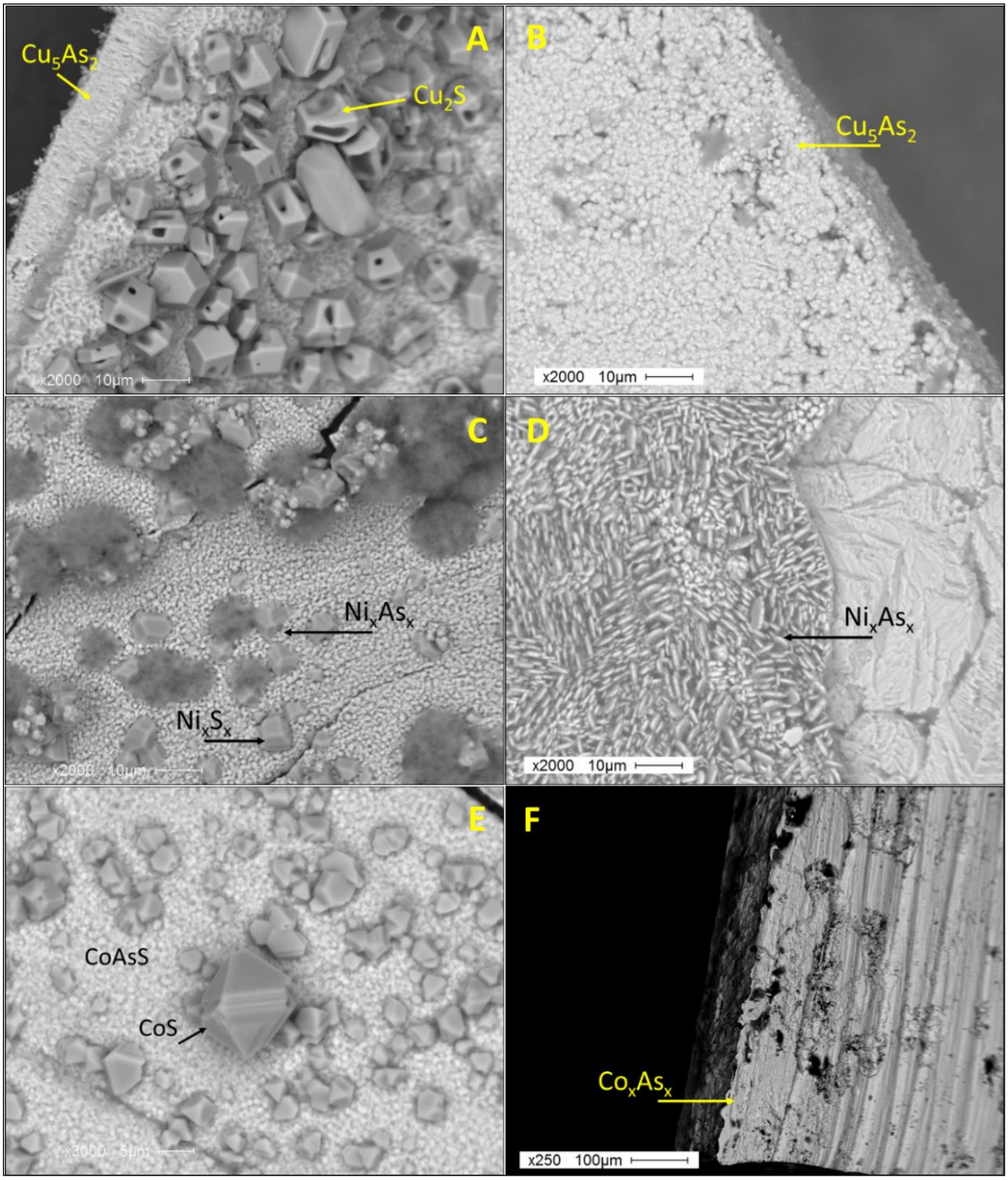

Figure 24. Summary of type B SEM images displaying total elemental foil replacement by arsenides with overgrowths of sulfides (300°C) or arsenide growth with no sulfide overgrowth textures (150°C). (A) Cu 300°C, (B) Cu 150°C, (C) Ni 300°C, (D) Ni 150°C, (E) Co 300°C, and (F) Co 150°C.

The main reason for the relative lack of TAR and TSR in the type C experiments compared to the types A and B experiments is likely due to the pH of the solutions (pH ~ 4 in type C compared to pH < 2 in types A and B). For example, Ohmoto and Lasaga (1982) showed that the rate of chemical and isotopic equilibrium between aqueous sulfate and sulfide at elevated temperature (100 to 300°C) is much faster at low pH (<2) than at high pH. This could help explain why sulfate was reduced to sulfide in many of the type A and B experiments, but not in the type C experiments. By analogy, it is possible that redox equilibrium between different dissolved arsenic species is also much faster at low pH compared to high pH. If so, this would help explain why TAR occurred in most of the type A and type B experiments, but only at 250°C or 300°C in the type C experiments, and to a much lesser extent.

Because of the low pH, it is probable that corrosion of the metal foils in the type A and B experiments would have created a high partial pressure of $H_2(g)$ by a dissolution reaction such as the following, where Me = metal foil:

$$Me(s) + 2H^+ \rightarrow Me^{2+} + H_2(g) \quad (13)$$

Once formed, $H_2(g)$ could have helped to reduce sulfate to sulfide, or arsenite to arsenide, via reactions such as:

$$HSO_4^- + 4H_2(g) \rightarrow HS^- + 4H_2O \quad (14)$$

$$2As(OH)_3\,(aq) + 6H_2\,(g) \rightarrow 2H_3As\,(aq) + 6H_2O\,(l) \quad (15)$$

At the higher pH of the type C experiments, less metal corrosion via reaction (13) would have occurred, and consequently less production of $H_2(g)$. In the type A and B experiments, it is not known whether TAR or TSR occurred by direct reaction with the surface of the metal foil, or indirectly by reaction with $H_2(g)$ that evolved during corrosion of the foil. It is possible, for example, that the rapid conversion of the metal foil to metal-arsenides (Fig. 24) was a direct,

surface-controlled redox reaction. In contrast, the growth of metal-sulfides may have involved the slower reaction of dissolved sulfate with $H_2(g)$ to form H_2S or HS^-, and subsequent precipitation of metal-sulfides. This issue should be investigated further in future experiments.

4.2. Geologic Applications

In some hydrothermal deposits, such as the "five element suite" Co-Ni-As-Ag-Bi vein deposits of the Cobalt-Gowganda, Echo Bay, and Thunder Bay Districts of Canada, ore textures reveal a succession of early metal-arsenide rosettes of varying compositions overlain by later sulfide rimming and replacement (Petruk, 1971; Robinson and Ohmoto, 1973; Franklin et al., 1986). Similar textures are demonstrated by the type B experiments, which show a succession of arsenide to sulfarsenide to sulfide mineralization (Figure 24). In the specific environments that produce the "five element suite" ore deposits, the texturally defined successive minerals can be the result of TAR occurring more quickly within the temperature range 150-250°C.

Similar rimming and rosette textures have been observed in samples from other deposits. Samples from the Cobalt District in Ontario, Canada, showed dendritic silver grains surrounded by breithauptite (NiSb), and cobaltite (CoAsS) (Figure 25A; Craig and Vaughan, 1981). The silver grains were interpreted to be the earliest in series, with breithauptite and cobaltite being deposited at a later pulse of ore deposition (Craig and Vaughan, 1981). The presence of multiple phases of reduced As and S could be the product of simultaneous TAR and TSR occurring during the formation of these ores.

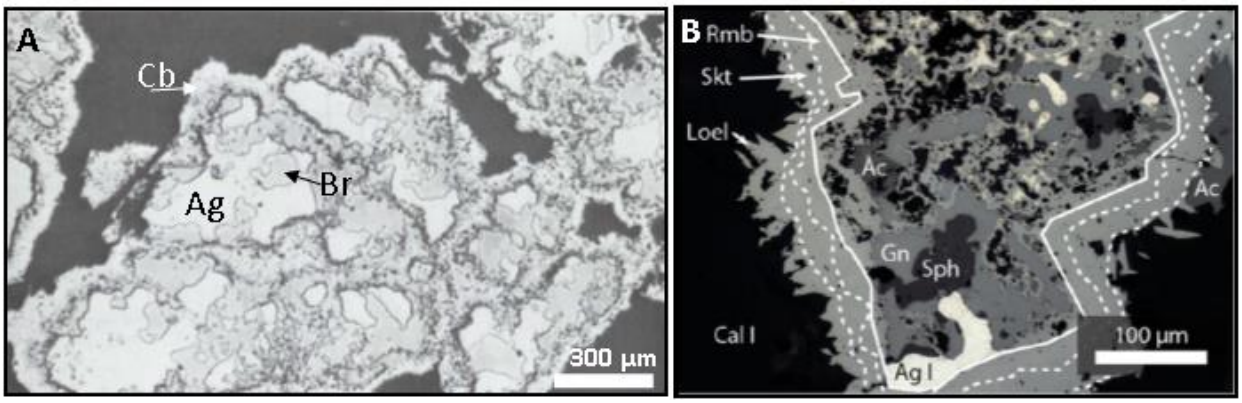

Figure 25. Arsenide minerals from ore deposits displaying rimming and rosette textures. A: Dendritic silver (Ag) surrounded by breithauptite (NiSb, Br), and cobaltite (CoAsS, Cb) from Cobalt, Ontario, Canada (modified from Craig and Vaughan, 1981. B: A once entirely silver mineral grain (Ag I) rimmed by rammelsbergite ($NiAs_2$, Rmb), skutterudite ($CoAs_3$, Skt), and löllingite ($FeAs_2$, Loel), then replaced by löllingite, acanthite (Ag2S, Ac), galena (PbS, Gn), sphalerite ((Zn,Fe)S, Sph), and calcite ($CaCO_3$, Cal 1), from Odenwald, SW Germany (modified from Burisch et al., 2017).

Figure 25B also shows an early Ag grain from a five-element suite deposit in Odenwald, Germany, surrounded by progressively As → S rich minerals (Burisch et al., 2017). The silver grain is rimmed by rammelsbergite ($NiAs_2$), skutterudite ($CoAs_3$), löllingite ($FeAs_2$), and then replaced by acanthite (Ag_2S), galena (PbS), sphalerite (ZnS), and calcite ($CaCO_3$) (Burisch et al., 2017). This can be summarized as native metals → arsenides → sulfides in order of deposition, if the texture is interpreted as pulses of evolving ore fluid precipitating insoluble minerals. In this specific deposit, it is suggested that methane gas was the active reducing agent and provides "far from equilibrium" conditions (Markl et al., 2016) to quickly produce native metals, arsenide minerals, and some sulfide minerals (Burisch et al., 2017). It is possible that the textures could not only be controlled by the introduction of arsenite-rich fluids and then later sulfate-rich fluids (spatially controlled), but by the differences in TAR and TSR reaction rates (temporally controlled).

As previously mentioned, another deposit type conducive to TAR and subsequent TSR is the Cobalt District, Ontario, Canada. A representative, simplified scenario drawn in Figure 26

shows how oxidized, briny fluids containing dissolved metals, like the previous scenario, can circulate around a hot, reduced intrusion. This circulating fluid would inevitably interact with other fluids derived from the reduced intrusion, and/or react with the heat of the intrusion to produce hydrogen gas (Equation 4). This would most likely occur near a structural control of fluid flow, like a fault, and form an ore body over time (Figures 3 and 26). The ore body would have stages of mineralization like those found in the experiments presented in this paper: TAR → TSR, or arsenide minerals → sulfide minerals (Figure 24).

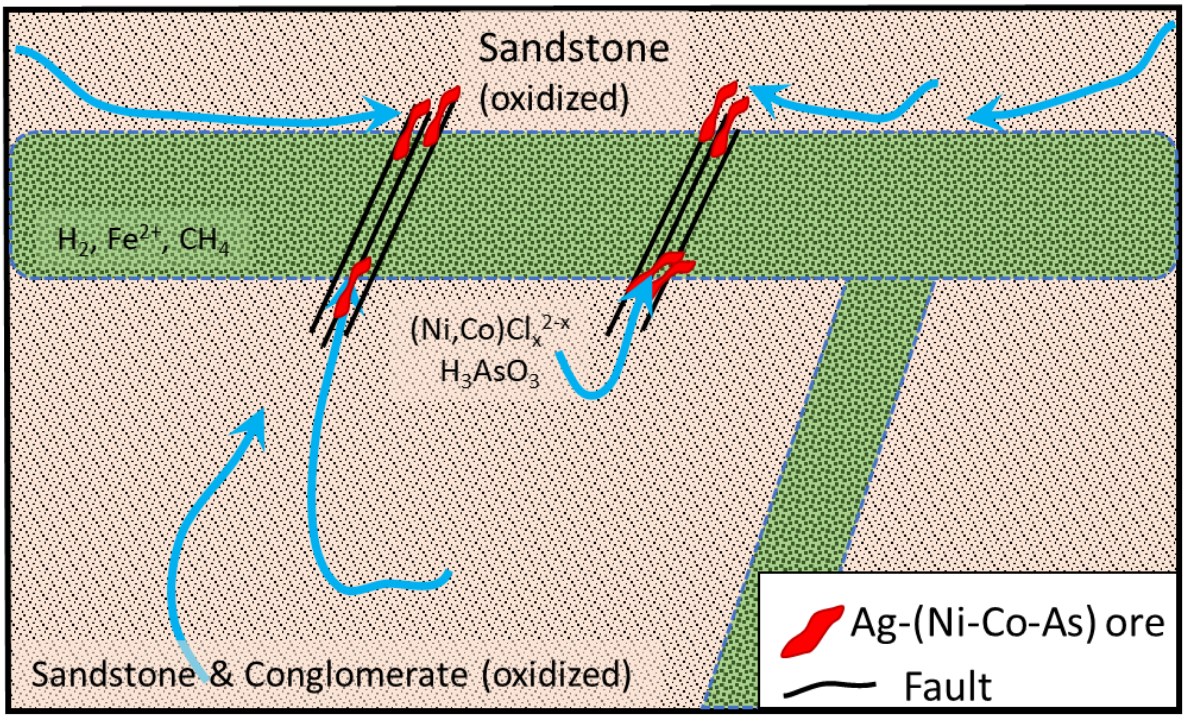

Figure 26. Simple schematic of the potential genesis of vein type Ag-Co-Ni-As deposits. This cartoon is inspired by the Cobalt District, Ontario, CA.

Figure 27 shows another scenario that has an ideal environment for TAR and TSR near a reducing front: an unconformity-type uranium deposit. In this scenario, moving, oxidized fluids chemically support the presence of oxidized forms of U, as well as Cu, Ni, and/or Co, and contain substantial concentrations of arsenite and sulfate. The moving, oxidized fluid could

interact with a more reduced environment by flowing through a fault system and mixing with fluids from a reduced formation. The underlying reduced rock is rich in hydrogen gas, ferrous iron, and/or organic carbon (e.g. methane), and after interaction with the oxidized fluids, would enable TAR, but not TSR to occur. The reaction products would successively deposit at the reduction zone, forming an orebody containing uraninite along with Ni-Co-arsenides, such as those found in the Athabaska Basin of Saskatchewan, Canada (Dahlkamp, 1978; Richard et al., 2013).

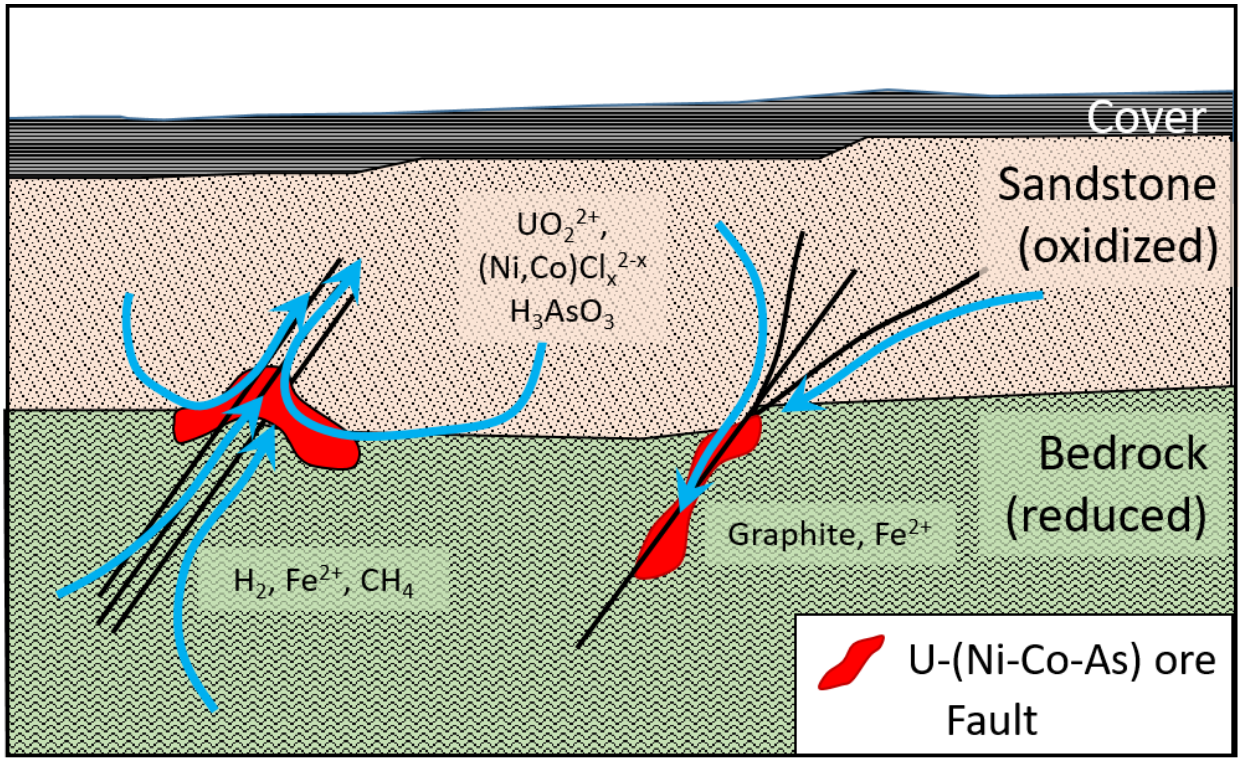

Figure 27. Simple schematic of a uranium unconformity type deposit. This shows how oxidized, briny metal-rich fluids can travel to a reduction zone to precipitate ore minerals, inspired by the Athabaska Basin, Saskatchewan, Canada.

An alternative explanation for the presence of unusually high concentrations of arsenide minerals in certain orebodies is that the original ore-forming fluids did not contain enough sulfate to form sulfide minerals when reduced. The absence of sulfate could force the system

into only precipitating arsenide or arsenide-like minerals. The absence of sulfate from the ore-forming fluids could be due to sulfate interacting with abundant ions in briny hydrothermal fluids, like calcium. As temperatures increase, the solubility of anhydrite ($CaSO_4$) decreases, which can result in anhydrite precipitating, thus removing sulfate (and calcium) from the fluid (Holland and Malinin, 1979). The precipitation of sulfate- and calcium-bearing minerals spatially distant from the higher temperature reduced zone would strip the fluid of a sulfur source before sufficient TSR temperatures could be reached.

5. Conclusions and Recommendations

5.1. Conclusions

Ore deposits found throughout various geologic settings contain textures displaying sulfide minerals surrounding arsenide minerals, which also surround native metals, to form conspicuous mineral rosettes. This ore texture, along with other, broader mineral and element distributions within mining districts, may be the result of thermochemical arsenite reduction taking place at a faster rate than thermochemical sulfate reduction. The results of this study confirm this hypothesis. Under strongly acidic experimental conditions, TAR occurred at a time-scale of days to weeks over the entire temperature range of 150 to 300°C, whereas TSR only occurred at $T \geq 250$°C. In the experiments where both TAR and TSR took place, textures indicate that TAR occurred first, by direct interaction of dissolved arsenite with the metal foils, whereas TSR happened more slowly, possibly through a reaction with $H_2(g)$ produced by corrosion of the foils. At higher pH conditions, TAR occurred to a minor extent at 250 and 300°C, whereas no TSR was noted.

An ore-forming fluid that is transporting Cu, Ni, and Co as chloride complexes along with sulfate and arsenite would be expected to precipitate arsenide minerals upon encountering a reduction boundary. If the concentration of total dissolved metal exceeds that of total dissolved As, then metal-sulfide minerals could form, but only after the arsenides were precipitated first. If the concentration of total dissolved As is greater than that of the metals, then sulfide minerals should not form, or should form only with metals (e.g., Zn, Pb) that do not readily combine with As to form arsenide minerals. Following these new ideas, ore-forming models for some well-known hydrothermal deposits containing Co-Ni-Cu arsenide minerals may need to be re-evaluated.

5.2. Recommendations for further work

In the experiments of this study, metal foils were used in excess to provide a very strong reducing buffer. The metal foils proved (mostly) successful in this regard, but some differences between them are noted. The Co foil, being the most expensive, was used in a somewhat miserly manner. The Co foil was of a much different shape, size, and texture than the other foils. The Co foil, because of its thickness, was cut into thin wires which were then shaped appropriately to keep them from falling into the solution when the tube was turned upright. The thicker wire shape could have affected the experiment in some manner, as the thick wire would have less surface area exposed in relation to its mass than the Ni and Cu foils (Cu foil being the thinnest). The surface finish of the Co foil was also not as smooth as the Cu or Ni foils. The Co foil had shallow surface striations like a brushed finish on stainless steel. The Ni and Cu foils had semi-mirror finishes, with Ni being matte and Cu being much more reflective, like common kitchen aluminum foil. The variable surface finish of these foils may have introduced another inconsistency that would affect reaction time, because smaller surface areas should slow reaction rates, as there would be a lesser difference in surface energy.

Solutions used to perform the experiments in this paper also varied considerably. Although the basic premise for each solution was similar, each experiment yielded different results, which could be related to the different solutions used. The solutions used in type A and B were more acidic ($pH < 2$) than the type C experiments ($pH \sim 4$), and arsenite availability within the type C solutions could have been impacted by the lack of HCl and Na^+ counter-ions somehow interacting with the solubilities of the minerals (Holland and Malinin, 1979). Future experiments could be designed in a way that maintains pH values more consistently and provides As(III) delivery to the system similarly to eliminate unnecessary variables.

The implementation of more native foils of varying compositions would help further characterize TAR. Easily obtainable candidates include: Fe, Ag, Bi, Sb, and other more common transition metals. Observing a larger swath of elemental foil compositions may provide further insight into specific mineral formation at low temperatures and help characterize other mineral textures seen in arsenide rich ore bodies.

A continuation of the basic experimental design to a broader range of temperatures and systematically varying the amounts of the reactants could be insightful. In the original experiments, metal foils of excess mass (supersaturated) were used to act as a strong buffer. A more in depth look at molar relationships between the foils and solutes could reveal a specific reaction otherwise overlooked.

Cross sectional SEM images of the foils would provide insight into reaction progress and give more detail in timed experiments as to how quickly these reactions may take place. With a cross sectional analysis, textures such as a “shrinking core”, or irregular corroded rinds could further characterize the TAR/TSR process, when using a substrate such as a cohesive foil versus other matrices, such as a nugget or grain. Measuring the reaction boundary and its progression throughout a timed experiment could provide quantifiable values to the reaction rate, instead of just comparative values relative to each process.

Results may benefit from performing these experiments on a larger scale, too. Increasing the mass of the foils and fluid may better demonstrate the rates of reactions and provide a viable avenue for reacting the fluids with actual rock samples. Using larger diameter tubes and an appropriate amount of solution would enable the experimentalist to use native silver ore or other analogous ores to act as the reductant, instead of metal foils. This would better mimic nature, albeit complicating the system. Textures and subsequent reactions were difficult to observe with

the naked eye at the scale of the experiments performed for this document. If larger pieces were used, perhaps more thorough observations could be noted, and samples more easily processed because their fragility would be less of a limiting factor.

6. References Cited

Avila-Salinas, W., 1990. Origin of the copper ores at Corocoro, Bolivia, in: Stratabound Ore Deposits in the Andes, Special Publication No. 8 of the Society for Geology Applied to Mineral Deposits. Springer, Berlin, Heidelberg, pp. 659–670. https://doi.org/10.1007/978-3-642-88282-1_52

Barton, L.L., Tomei, F.A., 1995. Characteristics and activities of sulfate-reducing bacteria, in: Sulfate-Reducing Bacteria, Biotechnology Handbooks. Springer, Boston, MA, pp. 228–230. https://doi.org/10.1007/978-1-4899-1582-5_1

Blair, T., 1997. Thermochemical arsenite reduction (TAR): a new hypothesis for the origin of "Cobalt-type" Ni-Co-arsenide vein deposits. Unpublished BS Thesis, McGill University 38.

Brown, A.C., 2006. Genisis of native copper lodes in the Keweenaw District, Northern Michigan: A hybrid evolved meteoric and metamophogenic model. Economic Geology 101, 1437–1444. https://doi.org/10.2113/gsecongeo.101.7.1437

Brunner, E., Woll, W., 1980. Solubility of sulfur in hydrogen sulfide and sour gases. Society of Petroleum Engineers Journal 20, 377–384. https://doi.org/10.2118/8778-PA

Burisch, M., Gerdes, A., Walter, B.F., Neumann, U., Fettel, M., Markl, G., 2017. Methane and the origin of five-element veins: Mineralogy, age, fluid inclusion chemistry and ore forming processes in the Odenwald, SW Germany. Ore Geology Reviews 81, 42–61. https://doi.org/10.1016/j.oregeorev.2016.10.033

Cox, D.P., Lindsey, D.A., Singer, D.A., Diggles, M.F., 2003. Sediment-hosted copper deposits of the world: Deposit models and database (Open-File No. 3.107). US Geological Survey.

Craig, J.R., Vaughan, D.J., 1981. Ore Microscopy and Ore Petrography, 2nd edition. ed. John Wiley & Sons, Inc.

Dahlkamp, F.J., 1978. Geologic appraisal of the Key Lake U-Ni deposits, northern Saskatchewan. Economic Geology 73, 1430–1449. https://doi.org/10.2113/gsecongeo.73.8.1430

Demergasso, C.S., Guillermo, C.D., Lorena, E.G., Mur, J.J.P., Pedrós-Alió, C., 2007. Microbial precipitation of arsenic sulfides in Andean salt flats. Geomicrobiology Journal 24, 111–123. https://doi.org/10.1080/01490450701266605

Escudero, L.V., Casamayor, E.O., Chong, G., Pedrós-Alió, C., Demergasso, C., 2013. Distribution of microbial arsenic reduction, oxidation and extrusion genes along a wide range of environmental arsenic concentrations. PLOS ONE 8. https://doi.org/10.1371/journal.pone.0078890

Franklin, J.M., Kissin, S.A., Smyk, M.C., Scott, S.D., 1986. Silver deposits associated with the Proterozoic rocks of the Thunder Bay District, Ontario. Can. J. Earth Sci. 23, 1576–1591. https://doi.org/10.1139/e86-148

Gammons, C.H., Yu, Y., Williams-Jones, A.E., 1997. The disproportionation of gold(I) chloride complexes at 25 to 200°C. Geochimica et Cosmochimica Acta 61, 1971–1983. https://doi.org/10.1016/S0016-7037(97)00060-4

Goldhaber, M.B., Orr, W.L., 1995. Kinetic controls on thermochemical sulfate reduction as a source of sedimentary H_2S, in: Geochemical Transformations of Sedimentary Sulfur, ACS Symposium Series. American Chemical Society, pp. 412–425. https://doi.org/10.1021/bk-1995-0612.ch023

Goldstein, T., Aizenshtat, Z., 1994. Thermochemical sulfate reduction a review. Journal of Thermal Analysis and Calorimetry 42, 241–290. https://doi.org/10.1007/BF02547004

Heinrich, C.A., Eadington, P.J., 1986. Thermodynamic predictions of the hydrothermal chemistry of arsenic, and their significance for the paragenetic sequence of some cassiterite-arsenopyrite-base metal sulfide deposits. Economic Geology 81, 511–529. https://doi.org/10.2113/gsecongeo.81.3.511

Holland, H.D., Malinin, S.D., 1979. The solubility and occurance of non-ore minerals, in: Hubert Lloyd Barnes (Ed.), Geochemistry of Hydrothermal Ore Deposits. 2nd Edition. John Wiley & Sons, Inc., pp. 461–508.

Jørgensen, B.B., Isaksen, M.F., Jannasch, H.W., 1992. Bacterial sulfate reduction above 100°C in deep-sea hydrothermal vent sediments. Science 258, 1756–1757. https://doi.org/10.1126/science.258.5089.1756

Kissin, S.A., 1992. Five-element (Ni-Co-As-Ag-Bi) veins. Geoscience Canada 19, 113–124.

Koenig, G.A., 1900. ART. XLII.--On Mohawkite, Stibio-domeykite, Domeykite, Algodonite and some artificial copper-arsenides: 1. Mohawkite. 2. Stibio-domeykite. 3. Mohawk Whitneyite. 4. Algodonite. American Journal of Science (1880-1910); New Haven 10, 439.

Ljunggren, P., Meyer, H.C., 1964. The copper mineralization in the Corocoro Basin, Bolivia. Economic Geology 59, 110–125. https://doi.org/10.2113/gsecongeo.59.1.110

Markl, G., Burisch, M., Neumann, U., 2016. Natural fracking and the genesis of five-element veins. Mineralium Deposita 51, 703–712. https://doi.org/10.1007/s00126-016-0662-z

Moore, P.B., 1962. Copper arsenides at Mohawk, Michigan. Rocks & Minerals 37, 24–26.

Ohmoto, H., Lasaga, A.C., 1982. Kinetics of reactions between aqueous sulfates and sulfides in hydrothermal systems. Geochimica et Cosmochimica Acta 46, 1727–1745. https://doi.org/10.1016/0016-7037(82)90113-2

O'Neill, H.S.C., Pownceby, M.I., 1993. Thermodynamic data from redox reactions at high temperatures. I. An experimental and theoretical assessment of the electrochemical method using stabilized zirconia electrolytes, with revised values for the Fe-"FeO", Co-CoO, Ni-NiO and Cu-Cu_2O oxygen buffers, and new data for the W-WO_2 buffer. Contributions to Mineralogy and Petrology 114, 296–314. https://doi.org/10.1007/BF01046533

Petruk, W., 1971. Mineralogical characteristics of the deposits and textures of the ore minerals. The Canadian Mineralogist 11, 108–139.

Richard, A., Cathelineau, M., Boiron, M.-C., Cuney, M., Mercadier, J., Rozsypal, C., Cauzid, J., Banks, D., Boulvais, P., Kendrick, M., 2013. Unconformity-related U deposits: recent advances from fluid inclusions and their host minerals, in: 12th Biennial SGA Meeting. Society for Geology Applied to Mineral Deposits, pp. 1575–1578.

Robie, R.A., Hemingway, B.S., Fisher, J.R., 1979. Thermodynamic Properties of Minerals and Related Substances at 298.15 K and 1 Bar (105 Pascals) Pressure and at Higher Temperatures. USGS Geological Survey Bulletin 1452.

Robinson, B.W., Ohmoto, H., 1973. Mineralogy, Fluid Inclusions, and Stable Isotopes of the Echo Bay U-Ni-Ag-Cu Deposits, Northwest Territories, Canada. Economic Geology 68, 635–656. https://doi.org/10.2113/gsecongeo.68.5.635

Thom, J., Anderson, G.M., 2008. The role of thermochemical sulfate reduction in the origin of Mississippi Valley-type deposits. I. Experimental results. Geofluids 8, 16–26. https://doi.org/10.1111/j.1468-8123.2007.00201.x

Tredoux, M., Zaccarini, F., Garuti, G., Miller, D.E., 2016. Phases in the Ni–Sb–As system which occur in the Bon Accord oxide body, Barberton greenstone belt, South Africa. Mineralogical Magazine 80, 187–198. https://doi.org/10.1180/minmag.2015.079.7.07

Xiao, Z., Gammons, C.H., Williams-Jones, A.E., 1998. Experimental study of copper(I) chloride complexing in hydrothermal solutions at 40 to 300°C and saturated water vapor pressure. Geochimica et Cosmochimica Acta 62, 2949–2964. https://doi.org/10.1016/S0016-7037(98)00228-2

7. Appendix A: SEM Spectra and Photographs

7.1. Type C experiments

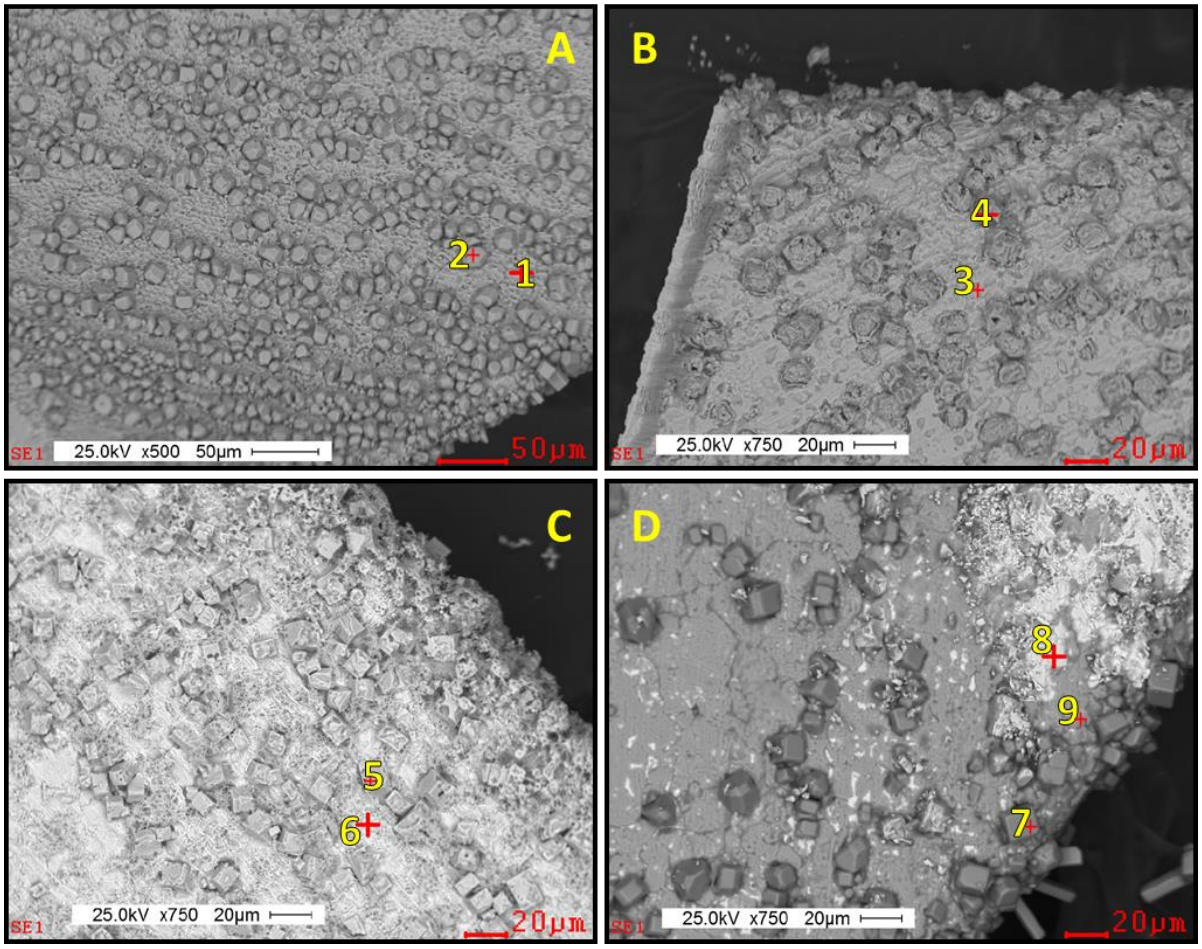

Table IV. Cu experiment at 300°C, A: one hour, B: five hours, C: one day, D: one week.

ID	atomic %		
	CuK	OK	SiK
1	100	-	
2	85.11	14.89	
3	100	-	
4	74.54	25.46	
5	73.44	26.56	
6	100	-	
7	41.38	14.12	44.5
8	100		
9	32.38	33.93	33.68

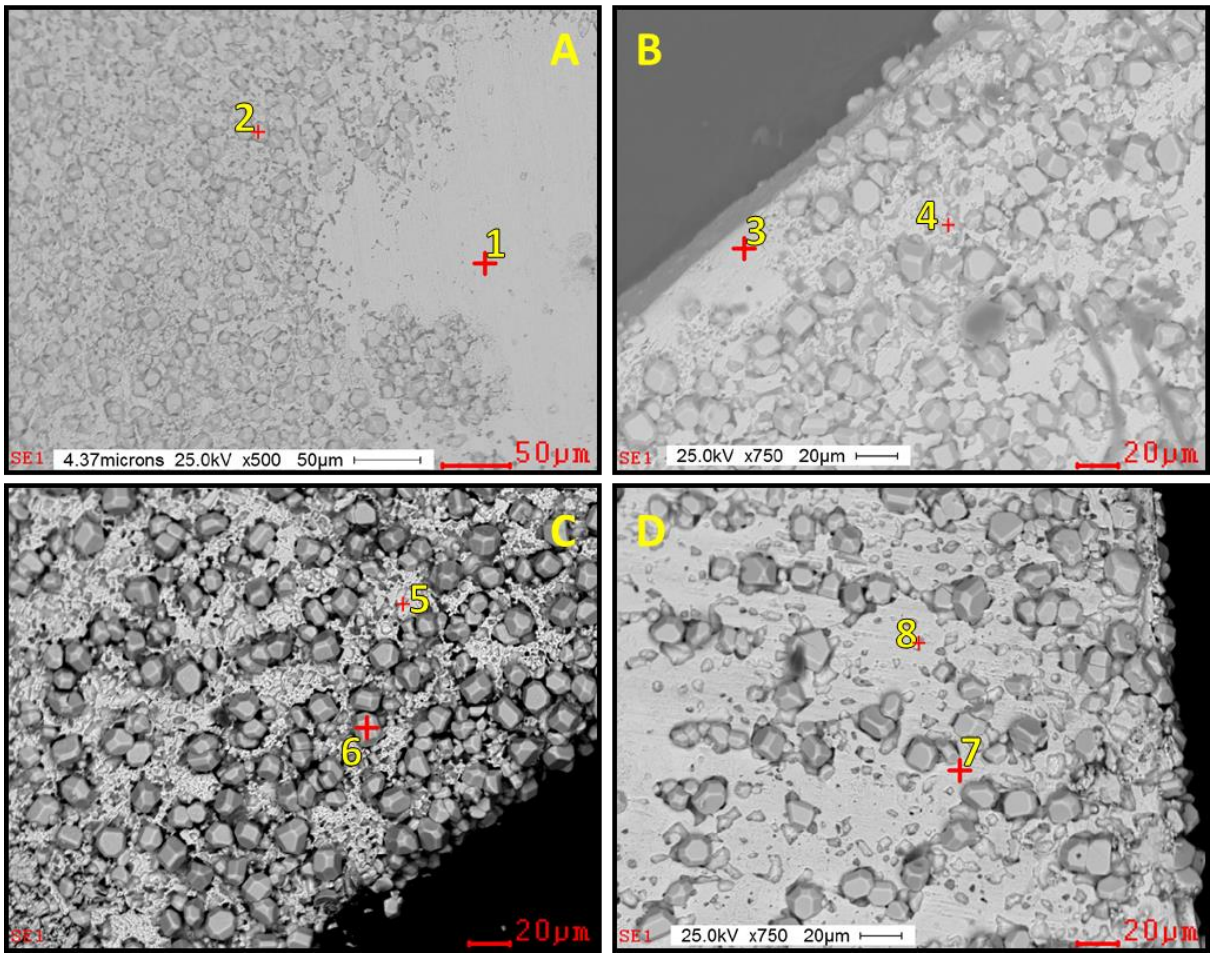

Table V. Cu experiment at 250°C, A: one hour, B: five hours, C: one day, D: one week

ID	atomic %	
	CuK	Ok
1	100	-
2	81.93	18.07
3	100	-
4	100	-
5	81093	18.07
6	100	-
7	100	-
8	81.93	18.07

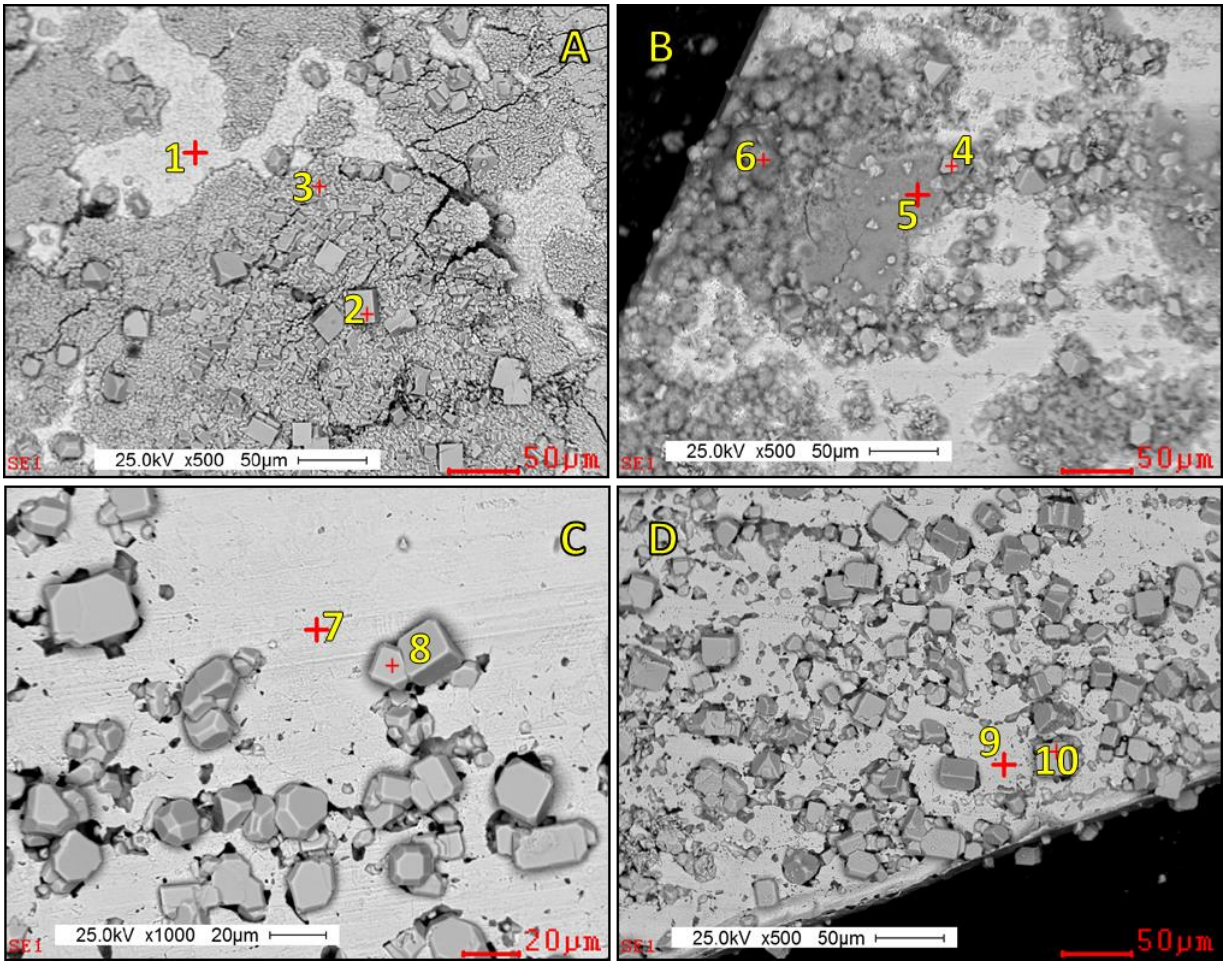

Table VI. Cu experiment at 200°C, A: one hour, B: five hours, C: one day, D: one week.

ID	atomic %			
	AsK	CuK	OK	SK
1		100		
2		78.97	21.03	
3		84.57	15.43	
4		84.26	15.74	
5	9.59	56.92	31.09	2.39
6	12.52	30.45	53.43	3.59
7		100		
8		94.72	18.13	
9		100		
10		83.08	16.92	

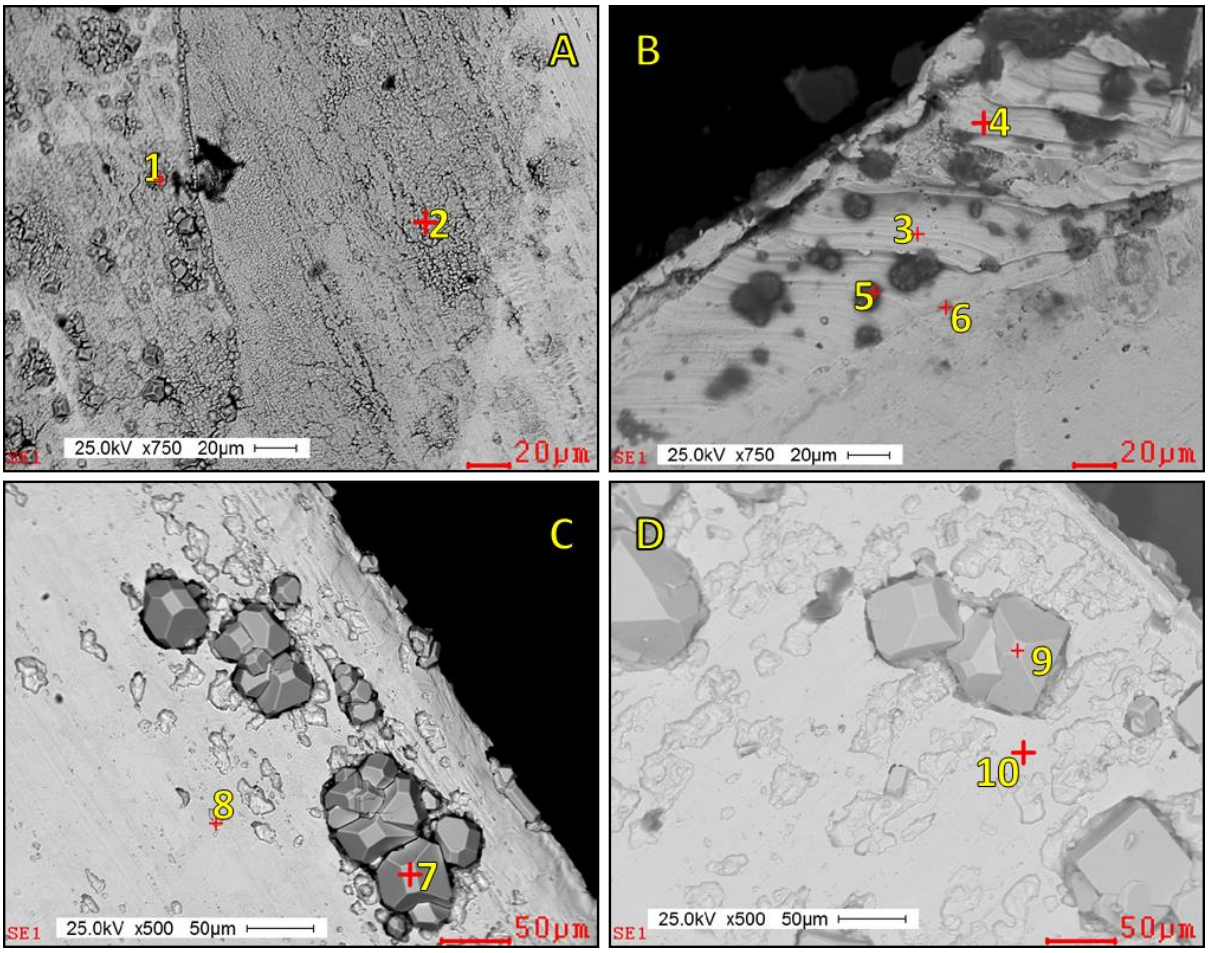

Table VII. Cu experiment at 150°C, A: one hour, B: five hours, C: one day, D: one week. *values obtained by the L shell.

ID	atomic %			
	AsK	CuK	OK	SK
1		87.41	12.59	
2		85.71	14.29	
3	4.01*	86.83	9.16	
4	5.58*	83.29	11.13	
5	4.29	12.99	70.33	15.22
6	5.98*	80.24	13.78	
7		84.19	15.81	
8		100		
9		82.67	17.33	
10		100		

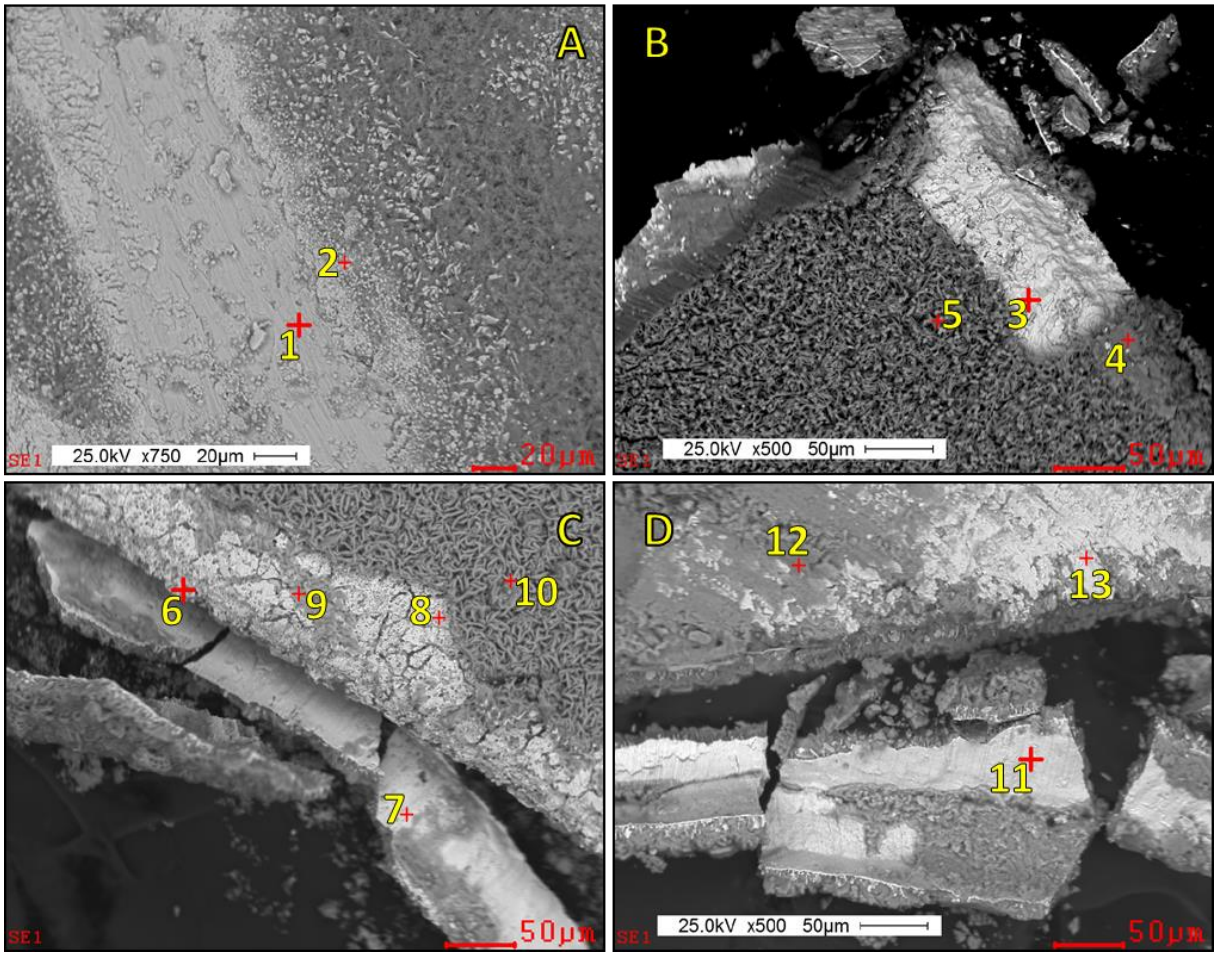

Table VIII. Ni experiment at 300°C, A: one hour, B: five hours, C: one day, D: one week. *values obtained by the L shell.

ID	atomic %				
	AsK	NiK	OK	SK	SiK
1		100.00			
2	19.12	55.53	22.73	2.61	
3		100.00			
4		23.10	48.94	0.73	27.19
5		17.22	60.91	1.61	20.26
6	2.36*	58.93	23.60	1.34	13.78
7	24.06	75.94			
8		77.59	16.38		6.03
9		47.17	30.07		22.76
10		15.16	58.17		26.66
11	20.94	60.02	13.43		5.6
12		32.11	34.96		32.93
13		83.27	10.66		6.08

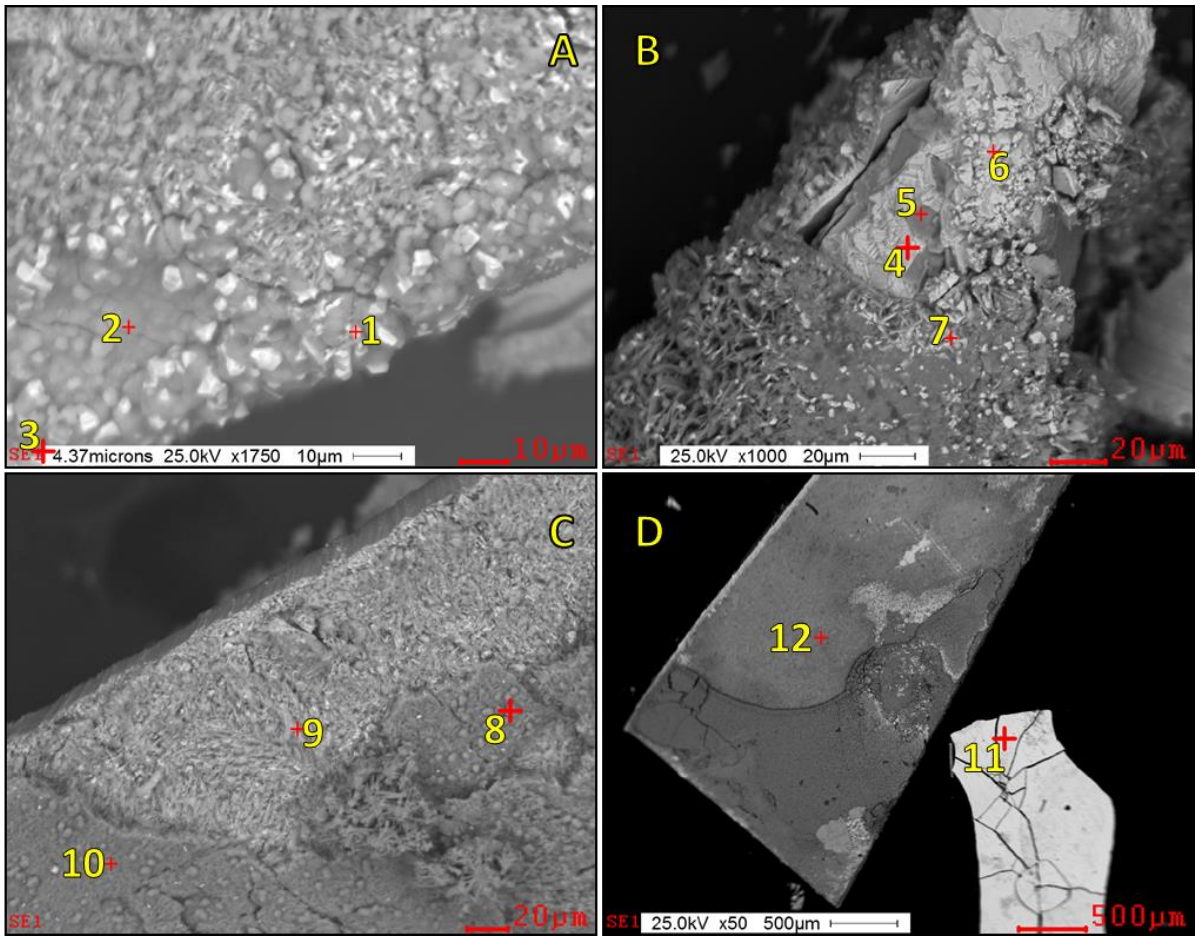

Table IX. Ni experiment at 250°C, A: one hour, B: five hours, C: one day, D: one week. *values obtained by the L shell.

ID	atomic %				
	AsK	NiK	OK	SK	SiK
1	23.90	65.21	10.89		
2	2.70	48.80	34.41	2.02	12.08
3	4.63	28.59	52.92	3.06	10.80
4		100.00			
5		84.44	7.73	7.83	
6	27.70	72.30			
7	17.58	52.08	26.84	3.49	
8	0.91*	22.96	50.89	1.09	24.16
9	13.53	48.69	27.63	2.27	7.88
10	23.36	67.41	6.11		3.12
11	28.2	71.8			
12		40.39	38.22		21.39

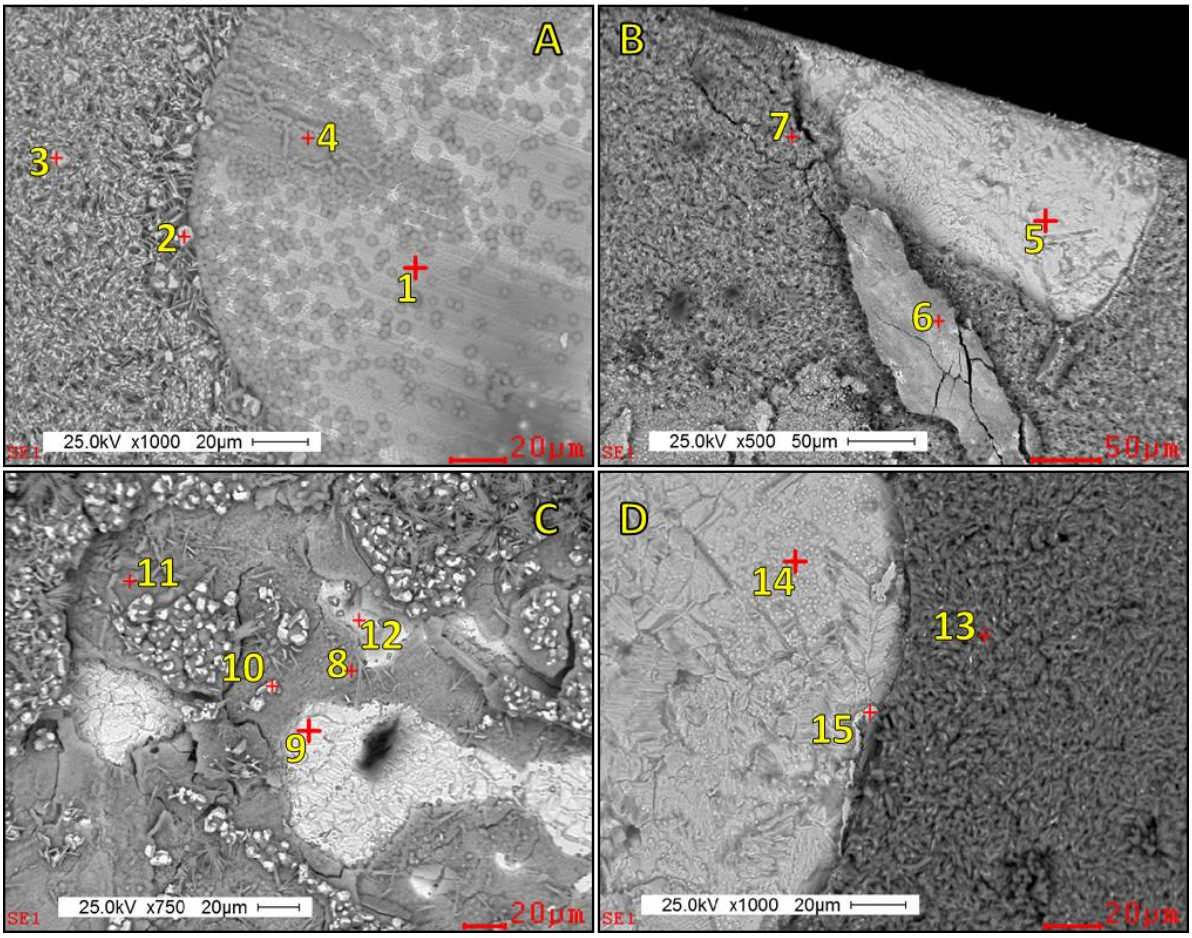

Table X. Ni experiment at 200°C, A: one hour, B: five hours, C: one day, D: one week. *values obtained by the L shell.

ID	atomic %				
	AsK	NiK	OK	SK	SiK
1	8.61*	81.28	10.12		
2	23.29	61.70	15.02		
3	20.55	54.66	24.79		
4	6.88	45.21	40.54	3.97	3.40
5	2.63*	85.42	11.95		
6	11.97	49.16	36.66	2.20	
7	8.59	38.69	43.48	1.73	7.51
8		53.70	28.45		17.85
9		91.72	8.28		
10	22.49	61.53	12.45		3.53
11		46.38	33.52	1.01	19.1
12		88.6	11.4		
13		33.29	38.68	0.82	27.21
14		100			
15	1.96*	81.25	12.87		3.92

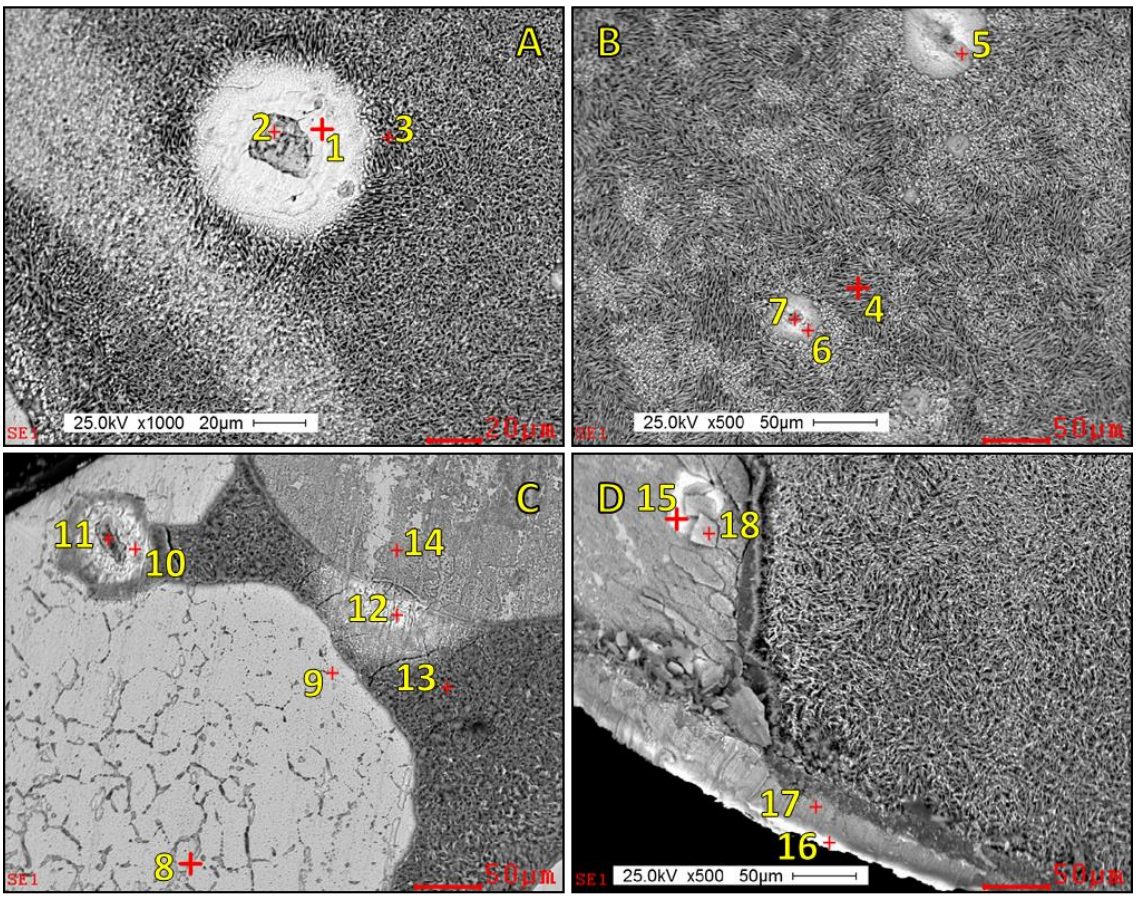

Table XI. Ni experiment at 150°C, A: one hour, B: five hours, C: one day, D: one week. *values obtained by the L shell.

ID	atomic %				
	AsK	NiK	OK	SK	SiK
1	20.15	71.41	8.44		
2		86.42	13.58		
3	16.89	54.59	26.74	1.16	
4	16.32	57.04	22.87	3.78	
5	6.73	54.93	35.93	2.41	
6	12.82	39.79	44.23	2.09	1.06
7	7.81	34.58	50.11	5.29	2.20
8		81.96	18.04		
9	2.19	84.10	13.71		
10	13.85	77.59	8.56		
11	5.45	37.63	42.79	0.73	13.4
12	20.37	69.65	9.98		
13	8.1	37	41.55		13.35
14		71.15	23.83		5.02
15		100			
16	4.89*	85.7	9.41		
17		77.61	18.52		3.87
18	2.45	34.15	44.36		19.04

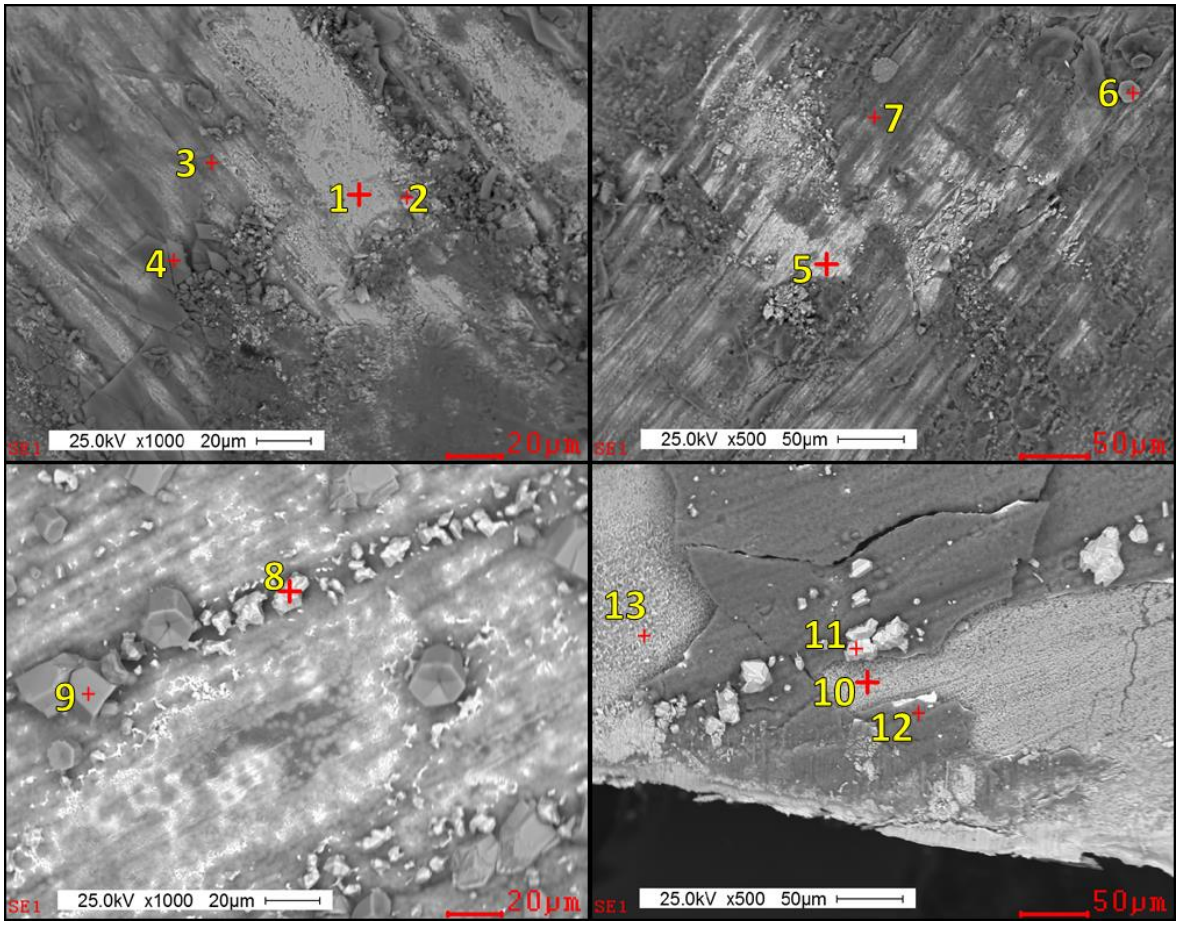

Table XII. Co experiment at 300°C, A: one hour, B: five hours, C: one day, D: one week.

ID	atomic %				
	AsK	CoK	OK	SK	SiK
1		100.00			
2	18.81	41.74	33.09	6.37	
3	6.54	33.62	48.26	9.46	2.12
4	2.93	33.33	50.38	12.17	1.19
5	23.95	59.43	16.62		
6	8.99	30.86	49.03	7.82	3.29
7	5.96	31.70	33.64	1.15	27.55
8	41.80	46.21	11.99		
9	9.88	26.57	57.49	6.06	
10		73.13	26.87		
11	40.66	46.4	9.53	3.41	
12		23.97	37.85		38.18
13	17.41	72.27	10.32		

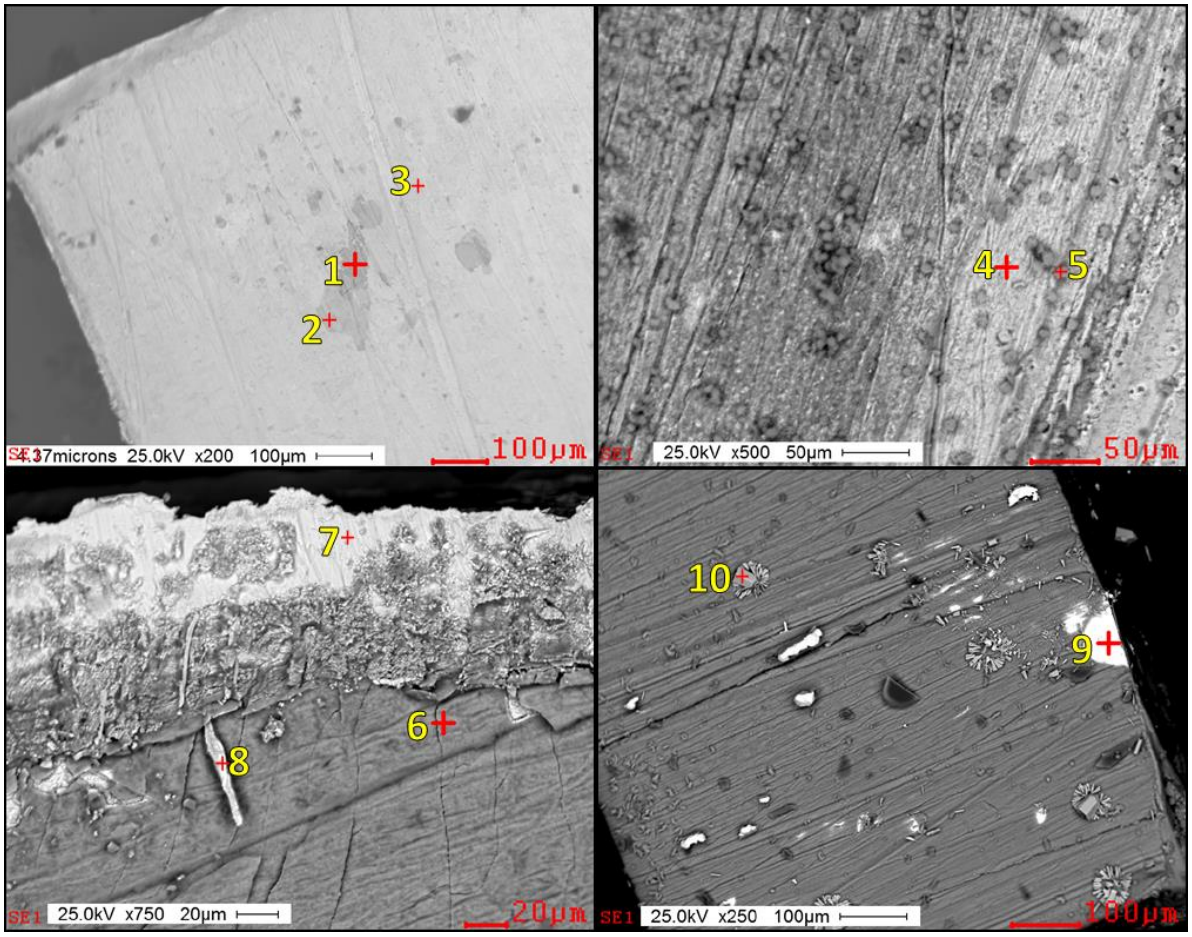

Table XIII. Co experiment at 250°C, A: one hour, B: five hours, C: one day, D: one week.

ID	atomic %				
	AsK	CoK	OK	SK	SiK
1	3.82	42.59	52.64	0.96	
2	4.01	55.09	40.90		
3	3.93	82.55	13.53		
4	22.00	31.04	34.66		12.29
5	3.66	22.63	54.80		18.91
6	9.71	33.63	35.89		20.77
7		100.00			
8	16.31	28.87	37.45		17.37
9	47.53	52.47			
10	12.3	32.76	47.35	5.17	2.41

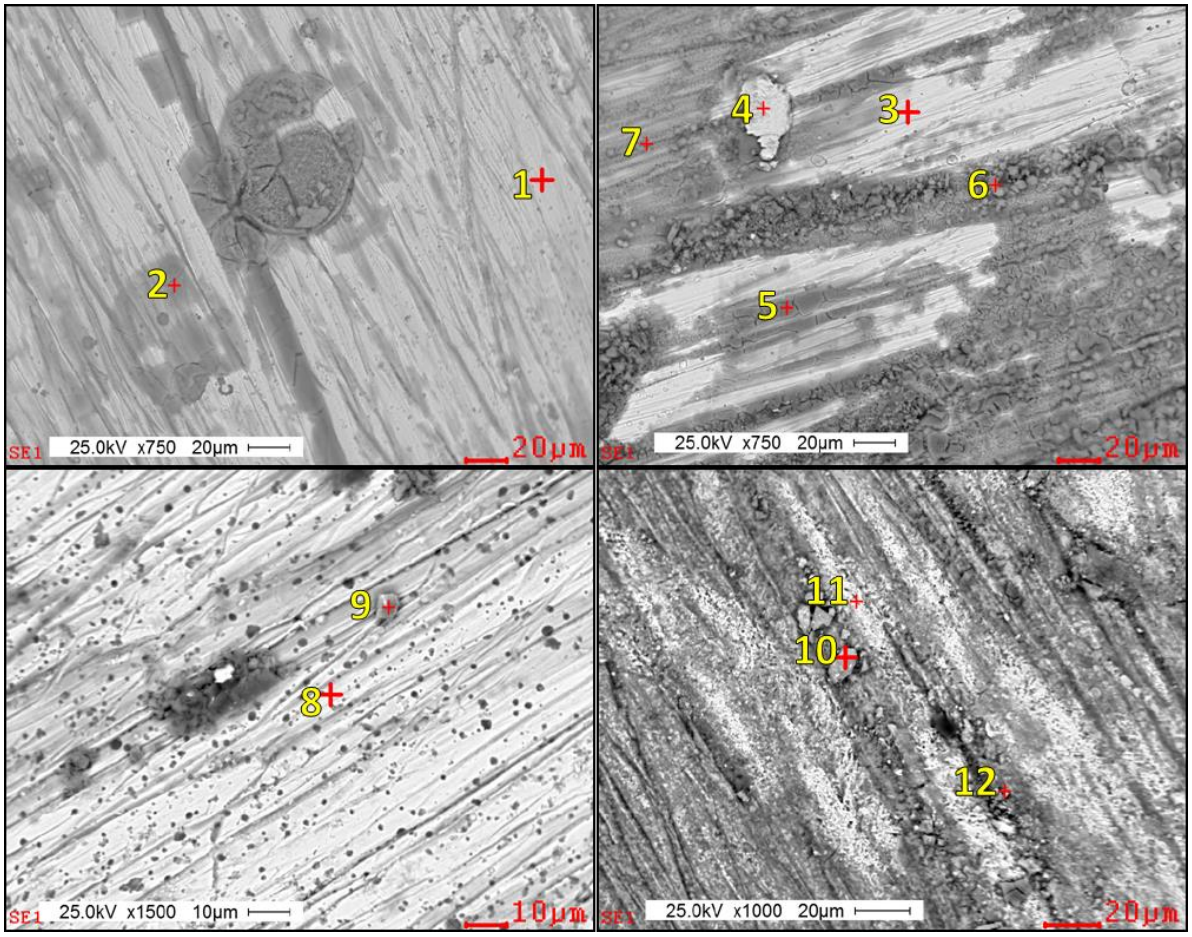

Table XIV. Co experiment at 200°C, A: one hour, B: five hours, C: one day, D: one week. *values obtained by the L shell.

ID	atomic %				
	AsK	CoK	OK	SK	SiK
1	5.36*	78.01	16.63		
2	1.92*	48.56	49.52		
3	4.54*	95.46			
4	4.62*	84.17	11.21		
5		49.43	45.60	4.97	
6	1.86*	54.39	38.80	4.95	
7	2.72*	34.76	59.04	3.47	
8	9.05*	90.95			
9	11.01	37.16	50.01	1.82	
10	11.23	52.42	33.59		2.75
11	5.69*	84.41	9.9		
12	6.51	64.57	25.06		3.85

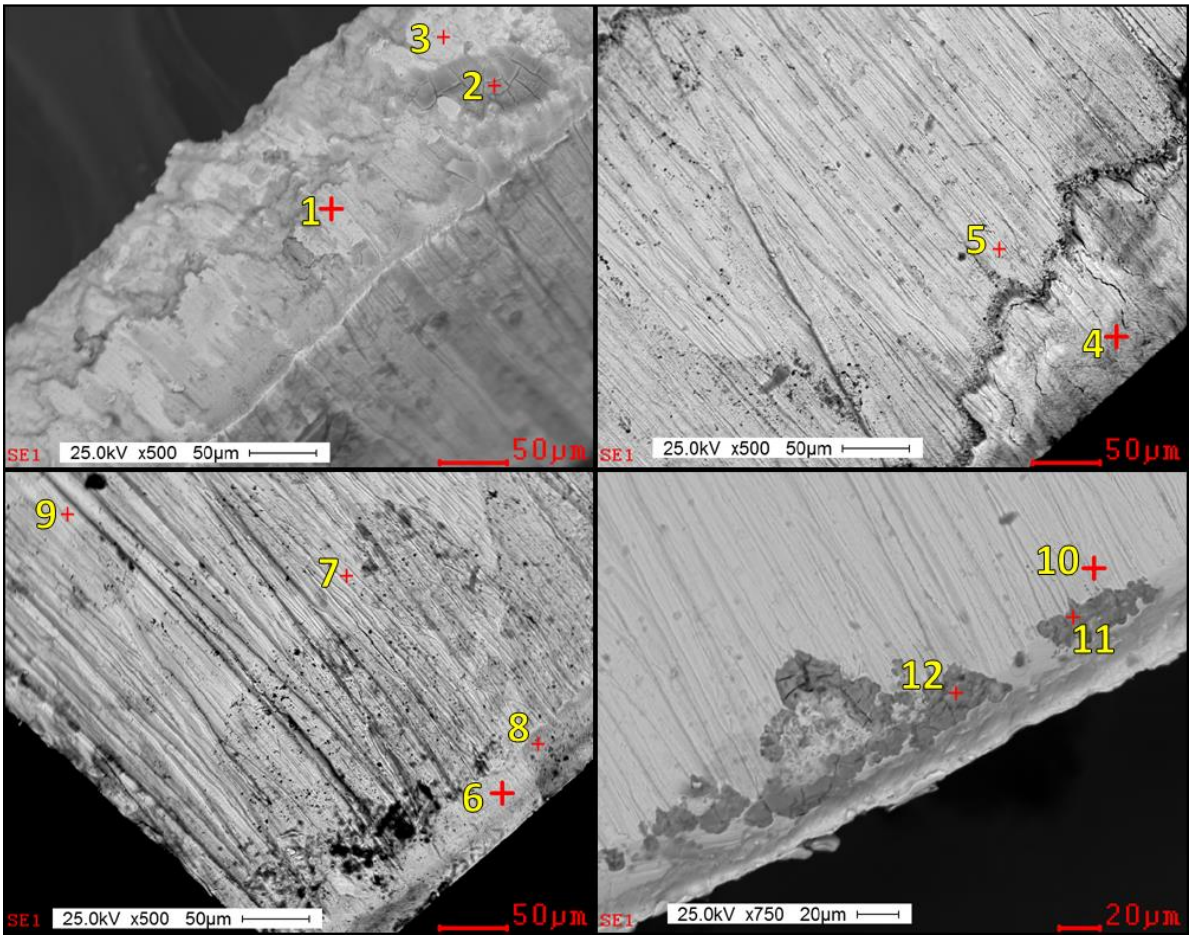

Table XV. Co experiment at 150°C, A: one hour, B: five hours, C: one day, D: one week. *values obtained by the L shell.

ID	atomic %				
	AsK	CoK	OK	SK	SiK
1	4.29	55.60	37.55	2.56	
2	3.45*	53.67	42.88		
3		67.88	32.12		
4	5.80	81.35	12.85		
5	7.93	80.62	11.45		
6	5.91	94.09			
7		100.00			
8	6.77*	68.78	24.45		
9		84.78	15.22		
10	3.72*	73.99	22.29		
11	1.79*	53.51	32.76	1.04	10.9
12	2.54	41.98	34.34	2.3	18.84

SIGNATURE PAGE

This is to certify that the thesis prepared by Nicholas C. Allin entitled "Experimental investigation of the thermochemical reduction of arsenite and sulfate: low temperature hydrothermal copper, nickel, and cobalt arsenide and sulfide ore formation" has been examined and approved for acceptance by the Department of Geological Engineering, Montana Technological University, on this 30th day of April, 2019.

Christopher Gammons, Ph.D, Professor
Department of Geological Engineering
Chair, Examination Committee

Glenn Shaw, Ph.D, Associate Professor
Department of Geological Engineering
Member, Examination Committee

Douglas Cameron, Ph.D, Professor
Department of Chemistry and Geochemistry
Member, Examination Committee

Gary Wyss, M.S., Laboratory/Equipment Specialist
Center for Advanced Mineral and Metallurgical Processing
Member, Examination Committee